AD NUMBER

ADB007022

NEW LIMITATION CHANGE

TO

Approved for public release, distribution unlimited

FROM

Distribution authorized to U.S. Gov't. agencies only; Test and Evaluation; Oct 1975. Other requests shall be referred to Air Force Rocket Propulsion Lab [DYSP], Edwards AFB, CA 93523.

AUTHORITY

AFRPL ltr dtd 24 Mar 1976

AEDC-TR-75-120

DEGRADATION OF LOW-SCATTER METAL MIRRORS BY CRYODEPOSIT CONTAMINATION

VON KÁRMÁN GAS DYNAMICS FACILITY
ARNOLD ENGINEERING DEVELOPMENT CENTER
AIR FORCE SYSTEMS COMMAND
ARNOLD AIR FORCE STATION, TENNESSEE 37389

October 1975

Final Report for Period January 1973 – December 1973

Prepared for

AIR FORCE ROCKET PROPULSION LABORATORY (DYSP)
EDWARDS AFB, CALIFORNIA 93523

NOTICES

When U. S. Government drawings specifications, or other data are used for any purpose other than a definitely related Government procurement operation, the Government thereby incurs no responsibility nor any obligation whatsoever, and the fact that the Government may have formulated, furnished, or in any way supplied the said drawings, specifications, or other data, is not to be regarded by implication or otherwise, or in any manner licensing the holder or any other person or corporation, or conveying any rights or permission to manufacture, use, or sell any patented invention that may in any way be related thereto.

Qualified users may obtain copies of this report from the Defense Documentation Center.

References to named commercial products in this report are not to be considered in any sense as an endorsement of the product by the United States Air Force or the Government.

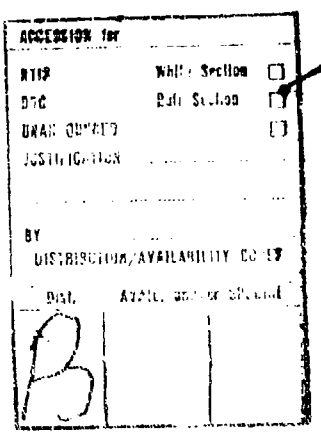

APPROVAL STATEMENT

This technical report has been reviewed and is approved for publication.

FOR THE COMMANDER

CARL J. SCHULZE
Major, USAF
Chief Air Force Test Director, VKF
Directorate of Test

CRAIG E. MAHAFFY
Colonel, USAF
Director of Test

REPORT DOCUMENTATION PAGE		READ INSTRUCTIONS BEFORE COMPLETING FORM
1 REPORT NUMBER AEDC-TR-75-128	2 GOVT ACCESSION NO.	3. RECIPIENT'S CATALOG NUMBER
4 TITLE (and Subtitle) DEGRADATION OF LOW-SCATTER METAL MIRRORS BY CRYODEPOSIT CONTAMINATION.		5 TYPE OF REPORT & PERIOD COVERED Final Report, January [illegible]-December [illegible]973 6 PERFORMING ORG. REPORT NUMBER
7 AUTHOR(s) Frederick Arnold, ARO, Inc.		8 CONTRACT OR GRANT NUMBER(s)
9 PERFORMING ORGANIZATION NAME AND ADDRESS Arnold Engineering Development Center (XO) Arnold Air Force Station, Tennessee 37389		10 PROGRAM ELEMENT, PROJECT, TASK AREA & WORK UNIT NUMBERS Program Element 62302F ~~Project~~ 5730
11 CONTROLLING OFFICE NAME AND ADDRESS Air Force Rocket Propulsion Laboratory (DYSP), Edwards AFB, California 93523		12 REPORT DATE October 1975 13 NUMBER OF PAGES 58
14 MONITORING AGENCY NAME & ADDRESS (if different from Controlling Office)		15 SECURITY CLASS. (of this report) UNCLASSIFIED 15a DECLASSIFICATION DOWNGRADING SCHEDULE N/A

16 DISTRIBUTION STATEMENT (of this Report)
Distribution limited to U.S. Government agencies only; this report contains information on test and evaluation of military hardware; October 1975; other requests for this document must be referred to Air Force Rocket Propulsion Laboratory (DYSP), Edwards AFB, California 93523.

17 DISTRIBUTION STATEMENT (of the abstract entered in Block 20, if different from Report)

18 SUPPLEMENTARY NOTES

Available in DDC

19 KEY WORDS (Continue on reverse side if necessary and identify by block number)

degradation
optical surface quality
mirror surfaces
contamination
particulate materials
infrared equipment
measurement
oxygen
carbon dioxide
deposition

20 ABSTRACT (Continue on reverse side if necessary and identify by block number)

Cryogenically cooled, low-scatter mirrors are currently in use or planned for use in space applications. An experimental investigation was made to determine the effect of condensed gases on the bidirectional reflectance distribution function (BRDF) of metal mirrors cooled to cryogenic temperatures. Such cryodeposits may develop from control rocket plumes and component outgassing as well as atmospheric contamination. An infrared scatter

over

DD FORM 1 JAN 73 1473 EDITION OF 1 NOV 65 IS OBSOLETE

20. ABSTRACT (Continued)

instrument system was developed for in situ measurement of the test mirror BRDF at 10.6-(μm) wavelength, and a molecular beam was used to provide a well-defined gas source for condensation on the test mirror. Both single species and mixtures were investigated at mirror temperatures from 20°K to 77°K. Oxygen and carbon dioxide deposits caused some increase in scatter, but the most catastrophic failure occurred when a cryodeposit shattered or crystallized. Conditions necessary for removal of cryodeposits are also described.

PREFACE

The work reported herein was conducted by the Arnold Engineering Development Center (AEDC), Air Force Systems Command (AFSC), at the request of the Air Force Rocket Propulsion Laboratory (AFRPL) under Program Element No. 62302F, Project 5730. The results of the tests were obtained by ARO, Inc. (a subsidiary of Sverdrup & Parcel and Associates, Inc.), contract operator of AEDC, AFSC, Arnold Air Force Station, Tennessee, under ARO Project No. V41V-02A (VA071) (VT0181). The author of this report was Frederick Arnold, ARO, Inc. Data reduction was completed in December 1973, and the manuscript (ARO Control No. ARO-VKF-TR-75-53) was submitted for publication on May 6, 1975.

CONTENTS

		Page
1.0	INTRODUCTION	7
2.0	APPARATUS	
	2.1 Test Chamber	8
	2.2 Molecular Beam	9
	2.3 Test Mirror	11
	2.4 Deposition Thickness Monitor	11
	2.5 Mirror Scatter Measurement	12
	2.6 Other Instrumentation	14
3.0	MIRROR SCATTERING MEASUREMENTS	
	3.1 Bidirectional Reflectance Distribution Function (BRDF) Calculations	16
	3.2 System Parameters for BRDF Measurement	18
4.0	TEST PROCEDURES	
	4.1 Preliminary Equipment Tests	19
	4.2 Mirror Scatter Measurement	21
	4.3 Cryodeposit Deposition	23
	4.4 Range of Test Conditions	24
	4.5 Factors Affecting the Data	24
5.0	RESULTS AND DISCUSSION	
	5.1 Bare Mirror Data	25
	5.2 Nitrogen-Directed Incidence	26
	5.3 Oxygen-Directed Incidence	26
	5.4 Carbon Dioxide-Directed Incidence	31
	5.5 Ammonia-Directed Incidence	36
	5.6 Carbon Monoxide, Water Vapor, and Air-Directed Incidence	39
	5.7 Mixtures-Directed Incidence	40
	5.8 Nitrogen and Oxygen-Random Incidence	41
6.0	SUMMARY OF RESULTS	
	6.1 Bare Mirror Data	41
	6.2 Scatter From Well-Behaved Cryodeposits	42
	6.3 Correlation of Visual Appearance with IR Scatter	42
	6.4 Shattering of Cryodeposits	42
	6.5 Effects of Mixtures	43
	6.6 Requirements for Cleanup	43
	REFERENCES	44

ILLUSTRATIONS

Figure		Page
1.	IR Scatter Test Configuration, 4 by 10-ft Chamber	8
2.	Test Chamber	9
3.	Molecular Beam Assembly	10
4.	Thickness Monitor Optical Schematic	12
5.	Chamber Test Section	13
6.	Mirror Temperature Calibration	15
7.	Laser Filter Box Output Distribution	20
8.	Telescope Field of View	22
9.	Clean Mirror Baseline, Logarithmic	27
10.	Clean Mirror Baseline, Semilogarithmic	28
11.	Effects of Partial Vaporization, N_2	29
12.	O_2 Runs 75 through 78	30
13.	O_2 Runs 166 through 169	31
14.	O_2 Runs 42A through 49	32
15.	O_2 Runs 49 through 63	33
16.	CO_2 Runs 83 through 86	34
17.	CO_2 Runs 91 through 93	34
18.	CO_2 Runs 95 through 99	35
19.	Cryodeposit, Run 108	36
20.	Cryodeposit, Run 109	37
21.	Cryodeposit, Run 110	38

TABLES

1.	Scatter Measurement, Raw Data Sample	45
2.	Range of Test Conditions	46

Page

3. Bare Mirror Scatter Measurements 47
4. N_2-Directed Flow Data. 51
5. O_2-Directed Flow Data 52
6. CO_2-Directed Flow Data 54
7. NH_3-Directed Flow Data 55
8. Directed Flow Data - CO, Air, and H_2O 56
9. Directed Flow Data - Mixtures 57
10. Random Incidence - N_2 and O_2 58

1.0 INTRODUCTION

The development of infrared sensors in recent years has led to use of cryogenically cooled optics to reduce background radiation. Further, the necessity of detecting small, low-intensity objects located close to large, intense objects has additionally required low-scatter optical surfaces.

The requirements of cryogenic cooling and low-scatter surfaces are not readily compatible, since a surface at less than 30°K will condense all incident gases except He, H_2, and Ne. Even at 77°K, most potential contaminants will condense. Such optics must always be under vacuum when cooled for launch or for ground testing and further protected from condensate by being the last elements cooled.

In spite of such precautions, contamination sources cannot be completely eliminated. For example, if a sensor is uncapped at 100 miles, with ambient pressure of 5×10^{-6} torr, cryodeposit formation could be as rapid as 0.05 microns per minute without consideration of the effects of sensor velocity or orientation. Other sources of contamination are the control rockets used to position the vehicle and the outgassing from sensor and vehicle components.

From a systems viewpoint, the entire sensor contamination problem can be divided into three areas of concern: (1) contaminant generation and transport, (2) effects of contamination on individual components, and (3) effects of component changes on sensor system performance. The current work addresses the second area and endeavors to provide information on the optical effects of cryodeposits of gaseous contaminants on low-scatter, cooled metal mirrors.

The work is comprised of two parts. The first consisted of spectral reflectance measurements in which the decrease in reflectance due to absorption and optical interference as a function of wavelength was determined at the specular angle for near normal incidence. These measurements are generally useful in determining changes in optical throughput caused by contaminant cryodeposits. This work has been completed and published (Refs. 1 and 2). The current work consists of off-specular reflectance measurement in which the increase in diffuse reflectance, or change in bidirectional reflectance distribution function (BRDF) due to scattering from condensates on the mirror surface is determined.

The design of most sensors is such that contaminant gases from outside the sensor will arrive at the primary optical surfaces at near normal incidence. In the current work, a molecular beam gas source was used in order to provide a well-defined and controllable contaminant gas flux at normal incidence. Contaminant gases studied included expected rocket plume, atmospheric, and outgassing components, both singly and in mixtures. The scattering effects were measured in situ by comparing the BRDF of the contaminated mirror with that of a clean mirror. The BRDF of the clean mirror was established by a series of measurements at ambient conditions and also at test conditions.

The work was sponsored by the Air Force Rocket Propulsion Laboratory (AFRPL) as part of the Sensor Degradation Program.

2.0 APPARATUS

2.1 TEST CHAMBER

The test chamber is a 3-1/2-ft-diam by 10-ft-long stainless steel vacuum tank equipped with a 6-in. baffled diffusion pump, a full cylindrical LN_2-cooled aluminum shroud, and a finned GHe-cooled (20°K) aluminum pumping section. The arrangement is shown in Fig. 1 along with a part of the test hardware. The chamber end flanges are removable for equipment installation, and the 4-ft-long test section of the

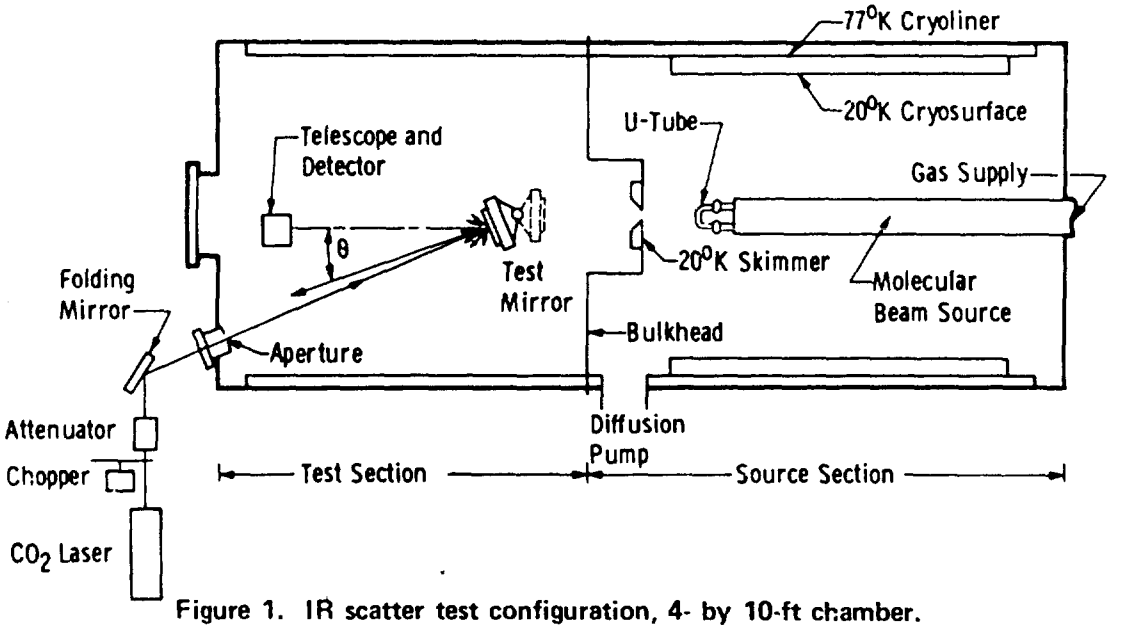

Figure 1. IR scatter test configuration, 4- by 10-ft chamber.

chamber is removable. The diffusion pump and molecular beam apparatus are attached to the 6-ft-long source section. A photograph of the test chamber with the end flange removed is shown in Fig. 2.

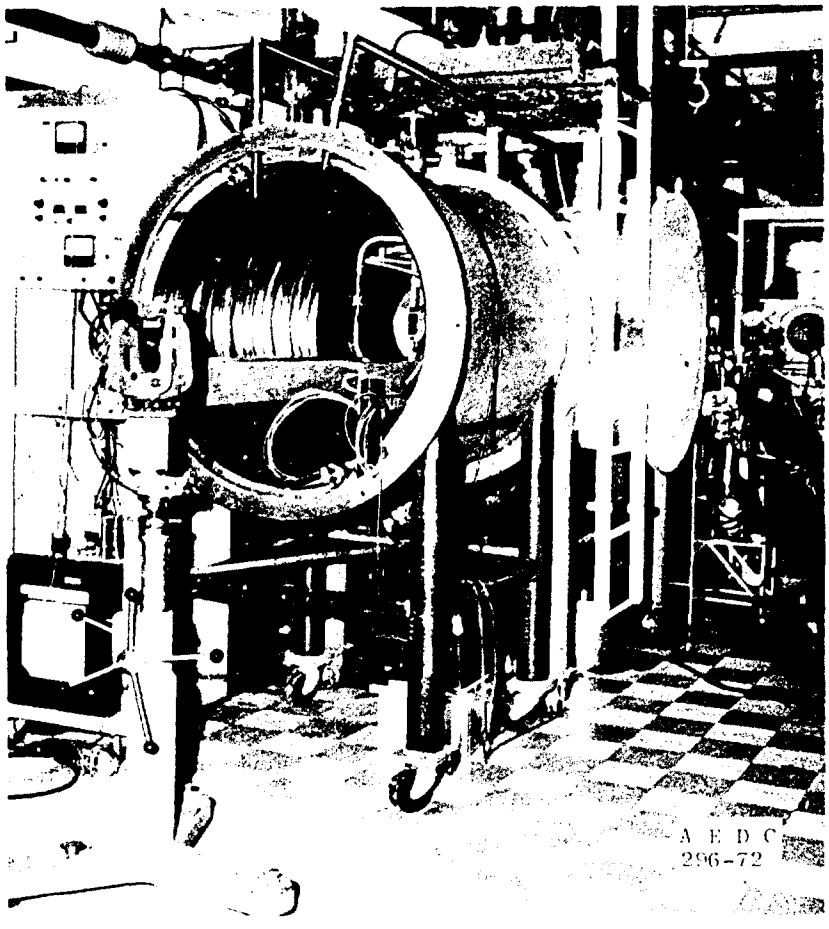

Figure 2. Test chamber.

2.2 MOLECULAR BEAM

A molecular beam source system was installed in the chamber to provide a geometrically defined and measurable gas flux on the test mirror. The beam source arrangement is identical to that described in Ref. 1. The chamber was separated into the source section and the test section by an aluminum bulkhead with a 14-in.-diam center opening between the chamber sections. A GHe-cooled (20°K) skimmer assembly (Fig. 3) was installed in the bulkhead opening. This skimmer assembly was also designed to provide 20°K cryopumping on the test section side,

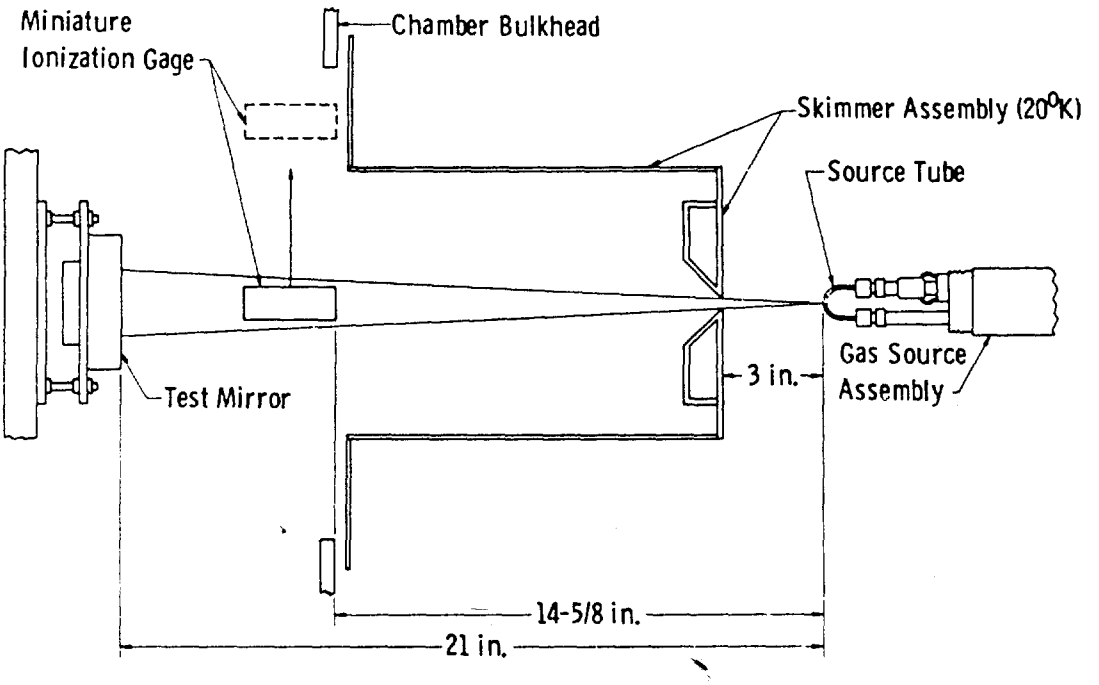

Figure 3. Molecular beam assembly.

and to allow passage of noncondensables from the test section to the diffusion pump in the source section. This was accomplished by allowing a narrow gap between the skimmer at 20°K and the bulkhead at approximately 300°K.

A water-cooled gas source assembly (Figs. 1 and 3) was inserted through the chamber end flange such that the linear position relative to the skimmer could be controlled externally. The source assembly was equipped with an electrically isolated platinum U-tube which could be directly heated from an external low-voltage power source. This U-tube contained a small orifice at the base of the U such that gas flowed from both ends of the tube toward the orifice. The free-jet expansion from the source was cryopumped in the source section, primarily on the skimmer, except for the central flow which passed through a 0.25-in.-diam opening in the skimmer. The resulting flux downstream of the skimmer opening formed a molecular beam which condensed on the cooled test mirror, forming deposits which simulate those expected on cooled optics of airborne or exo-atmospheric infrared sensors. References 3 and 4 describe previous molecular beam work at AEDC and also present capture coefficient data for some of the gases used in the current work.

The mass flux density at the mirror can be approximated analytically in order to determine the most convenient beam source dimensions and source pressure range. Reference 5 provides approximate angular flux distributions for free-jet expansions into vacuum as a function of specific heat ratio. The flux in a molecular beam skimmed from such an expansion (usually from a sonic orifice) is identical to that without the skimmer, provided the skimmer is located downstream of the transition to free molecular flow as it was in this case. The size of the desired beam then determines the skimmer diameter. Dimensions selected for the current work are shown in Fig. 3.

2.3 TEST MIRROR

The test mirror was a 2-in.-diam by 1-in.-thick low-scatter mirror, concave, with a 25-in. focal length. The surface consisted of "superpolished" nickel electrodeless plating on a 6061-T6 aluminum substrate. The mirror surface and quality are representative of state-of-the-art metal mirrors for use in IR sensors. Based on data provided by the supplier (Applied Optics Center, Burlington, Mass.), the reflectance at 10.6 μm is 0.90.

The mirror was bolted with an indium gasket to a GHe-cooled mounting plate which could be rotated from outside the vacuum chamber. Mirror temperature was controlled by throttling the 20°K GHe supply and allowing conduction through the mounting plate supports to raise mirror temperature. A 350-w heater was installed on the back of the mounting plate to facilitate evaporation of the cryodeposits from the mirror surface.

2.4 DEPOSITION THICKNESS MONITOR

Cryodeposit thickness was monitored during deposition using a He-Ne laser in a two-angle interference method (Fig. 4). The laser is split into two beams which are reflected onto the center of the test mirror when it is in deposition position. Two silicon solar cell detectors monitor the beams after reflection from the test mirror. The detectors were continuously recorded during deposition. Using the incident angles of the beams and the periods of oscillation of the detector outputs, the index of refraction and the thickness could be determined at the end of a deposit. Uniformity of the periods indicated a constant rate, and the rate was determined from total thickness over the measured deposition time. In

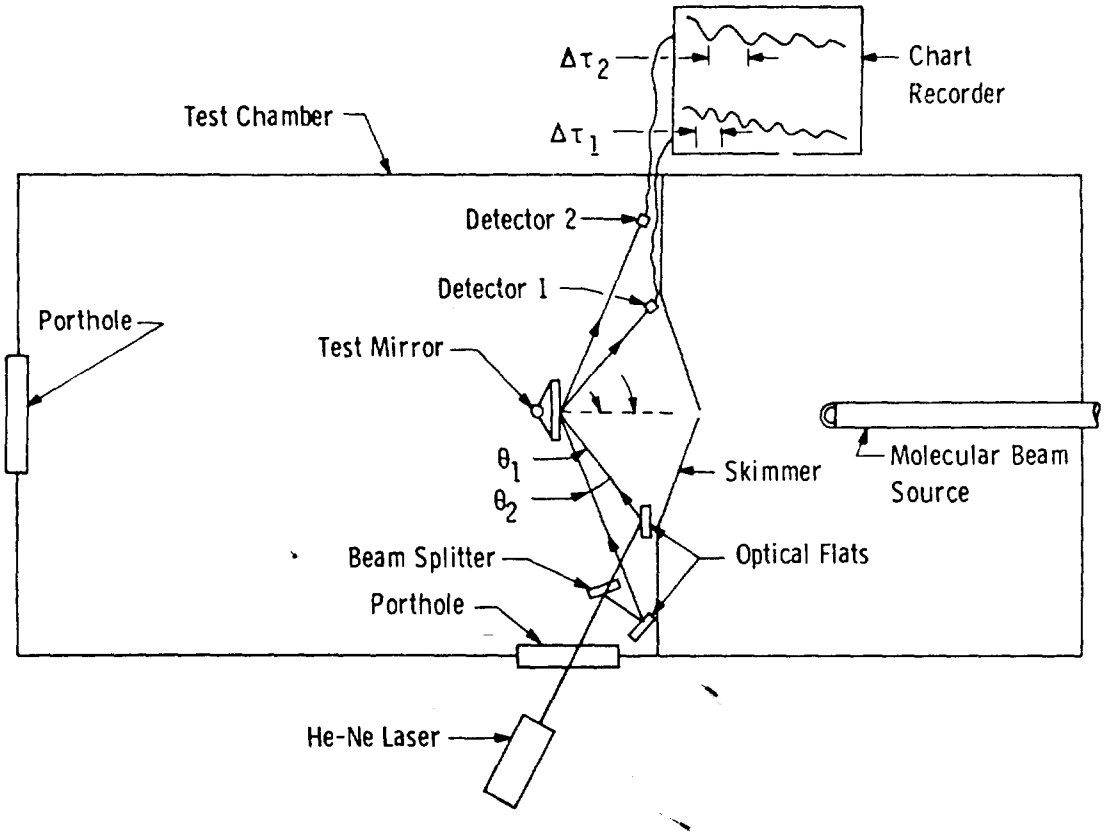

Figure 4. Thickness monitor optical schematic.

addition, after initial runs with a particular gas, the thickness corresponding to a cycle at either angle was known, and both thickness and rate could then be estimated during deposition. Alignment of the system was verified for each deposition by observing the laser beam on the solar cells through an observation port. The method is fully described and equations derived in Refs. 1 and 6.

2.5 MIRROR SCATTER MEASUREMENT

An optical schematic of the scatter measurement system is shown in Fig. 1. The optical system external to the chamber consisted of a 3-w CO_2 laser, 16-Hz chopper, beam attenuator, and positioning mirrors. The beam attenuator contained three reflective type attenuators with transmissions of 0.15, 0.0144, and 0.00661 in succession. Transmission range was thus from 1.0 (no filters) to 1.43×10^{-5} (all three filters). Two adjusting mirrors were used to translate and orient the

beam through the center of the chamber port and 0.4 in. field stop to the center of the test mirror. A thermopile detector mounted in a removable insert was used to verify that the beam was centered in the field stop. The window was a 2-in.-diam germanium flat, and the field stop was machined in the port on the vacuum side of the germanium.

The remainder of the scatter measurement system was located inside the chamber, with all components except the test mirror mounted on an aluminum plate for checkout and alignment outside the chamber. The test section installation is shown in Fig. 5. The pallet consisted of an infrared telescope assembly mounted on a remotely driven arm pivoted about the center of the test mirror. Angular position indicators were used to obtain the positions of the test mirror and the telescope arm. Drive motors also controlled the elevation position of the telescope assembly and the telescope mounting gimbal. Thus, the telescope could be remotely aimed at the mirror center and elevated to intercept the specular beam from the test mirror.

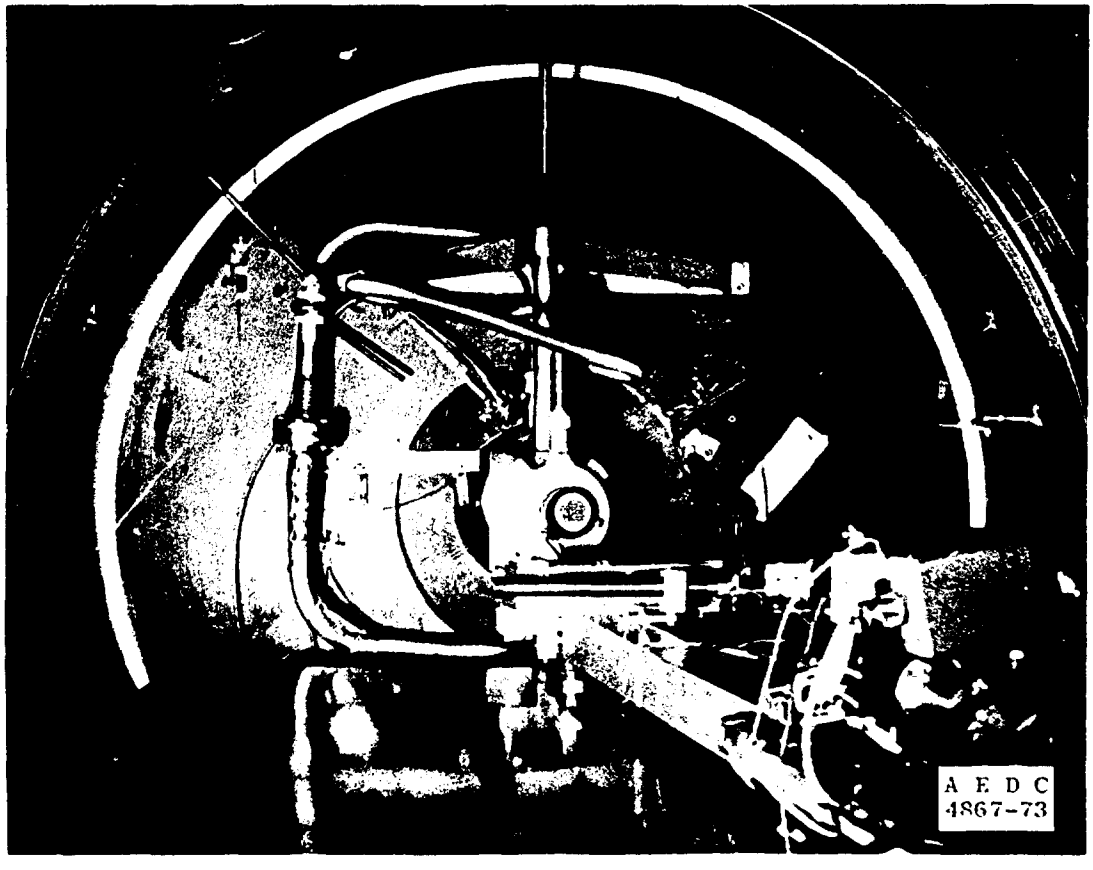

Figure 5. Chamber test section.

Two thermopiles inside the chamber were used to verify system alignment under test conditions. One was located behind the test mirror so that by rotating the test mirror 180 deg the thermopile occupied the exact position as the center of the test mirror. This was used to ensure that the incoming laser beam was striking the center of the test mirror. The other thermopile was mounted on the telescope horizontal centerline at a known angular separation from the center of the telescope lens. This was used to adjust telescope elevation so that the specular beam was on the horizontal centerline of the telescope.

Aiming of the telescope was the last alignment check and was accomplished by centering the specular beam on the center of the telescope lens and monitoring signal while moving each gimbal drive. The center was determined by timing the drives across the specular beam and taking the midpoint. This position corresponded with peak signal levels.

The telescope consisted of a 1-in.-diam by 2.5-in.-focal length germanium lens and a pyroelectric detector. The detector was a Barnes pyroelectric, 1 mm square, with a germanium window. Nominal responsivity of the detector was 2540 v/w, and the usable dynamic range was better than 10^5. All three germanium elements of the system (chamber port, telescope lens, and detector window) were antireflection coated for 10.6-μm wavelength radiation.

The detector signal was read out on a PAR HR-8 lock-in amplifier using a reference signal derived from the 16-He chopper. The minimum signal level that could be reliably measured was approximately 0.5 μv.

2.6 OTHER INSTRUMENTATION

In addition to cryodeposit thickness, mirror temperature and source gas stagnation conditions are required to define the cryodeposit. Of these, mirror temperature is most critical. A thermistor bolted directly to the test mirror with leads heat sunk to the GHe supply was used. An in-place calibration was obtained using deposition rate and gas vapor pressures. The calibration procedure is described in detail in Ref. 1, and the results for the thermistor used are shown in Fig. 6.

Source gas temperature was assumed equal to the source cooling water temperature for all cryodeposits made with an unheated source.

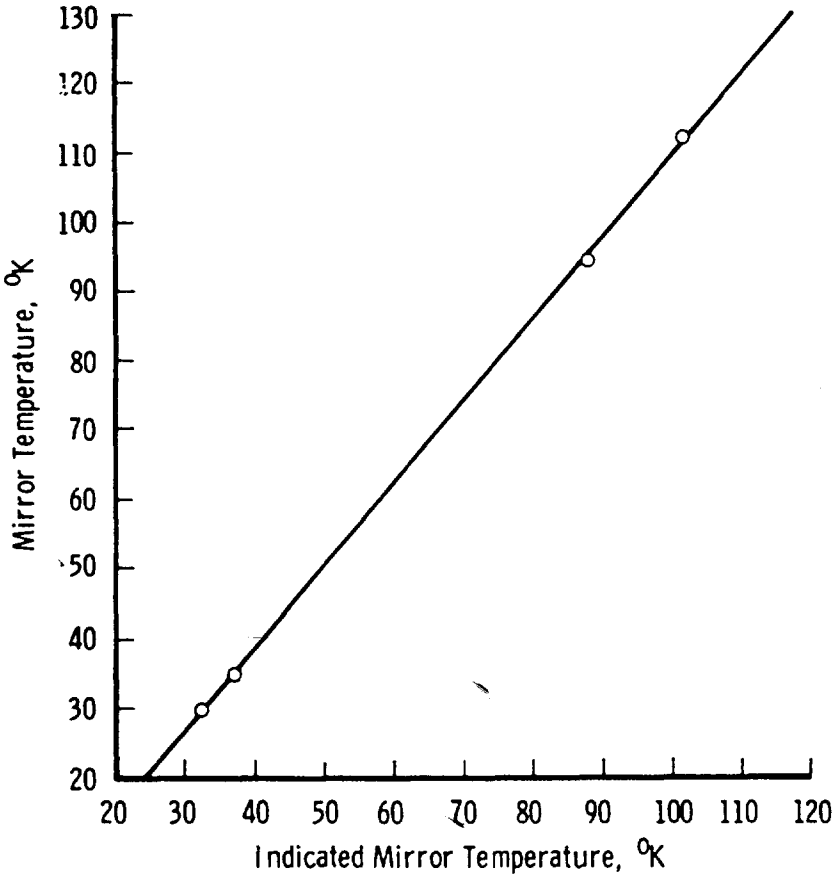

Figure 6. Mirror temperature calibration.

For heated source cryodeposits, the current and voltage applied to the source U-tube were measured, and the calibration with gas temperature for the work described in Ref. 1 was used.

Source stagnation pressure was read directly from a gage and was recorded from an independent transducer on a strip chart. Also recorded on the same strip chart during each deposition were the thickness monitoring solar cells, mirror temperature, chamber source section temperature, and chamber test section pressure.

3.0 MIRROR SCATTERING MEASUREMENTS

3.1 BIDIRECTIONAL REFLECTANCE DISTRIBUTION FUNCTION (BRDF) CALCULATIONS

The definition of BRDF used is

$$f_r(\theta_o, \phi_o; \theta_s \phi_s) = \frac{1}{L_o(\theta_o, \phi_o)} \frac{dL_s(\theta_s, \phi_s)}{\cos \theta_o d\Omega_o} \text{ / sr} \tag{1}$$

where radiance $L = \frac{1}{\cos \theta} \frac{\partial^2 \Phi}{\partial A \partial}$ w/m²-sr. (2)

Φ = power

A cos θ = projected surface area

ω = solid angle

Spherical Coordinate System

ϕ = longitude (azimuth)

θ = co-latitude (polar)

subscript o refers to incident beam

subscript s refers to scattered beam

Following Scheele (Ref. 6), assume collimated incident radiation from the (θ_O, ϕ_O) direction and further arbitrarily set the azimuth angle $\phi_O = \Pi$ (i.e., an isotropic scatterer). For these conditions it can be shown that

$$f_r(\theta_o; \theta_s, \phi_s) = \frac{I_s(\theta_s, \phi_s)}{\Phi_o} \tag{3}$$

That is, the BRDF as a function of incidence angle and position of scattering measurement is the scattered intensity (w/sr) divided by the incident power (w).

In the present case, laser energy is incident on a mirror much larger than the laser beam. An infrared telescope of entrance area A_D views an

area slightly larger than the irradiated area at a distance R which is much larger than either telescope aperture diameter or laser beam diameter.

The scattered power entering the detector system (i.e., the telescope) is

$$\Phi_s = I_s(\phi_s, \phi_s) \cdot \omega \tag{4}$$

where $\omega = A_D/R^2$ is the solid angle of reflected energy received by the telescope. Then

$$f(\theta_o;\theta_s,\phi_s) = \frac{\Phi_s/\omega}{\Phi_o} \tag{5}$$

For a low-scatter mirror, most of the reflected power will be contained within a small solid angle around the specular position. Thus, by using measured surface reflectivity at the wavelength of interest, we may calculate incident power from measured specularly reflected power. Thus,

$$\Phi_o = \frac{\Phi_s'}{\rho} \tag{6}$$

were $\Phi_{S'}$ is the power within some small solid angle about the specular angle and ρ is the mirror reflectivity at the wavelength of interest.

One additional refinement is necessary in order to overcome the inadequate dynamic range and power capability of available detectors. A set of calibrated filters in the main laser beam was used to attenuate the beam by known amounts. Thus F_S is the attenuation factor used for a scattering measurement and F_O is the attenuation used for measuring the incident power. For convenience, all measurements were referenced to an unattenuated beam; thus,

$$\Phi = F\bar{\Phi} \tag{7}$$

where $\bar{\Phi}$ is the power if the main beam were unattenuated. Now for a linear detector,

$$\Phi = kS \tag{8}$$

where S is detector signal and k is a calibration constant.

In order to relate the measurements to an unattenuated beam, the basic relation is written

$$f_r(\theta_o;\theta_s,\phi_s) = \frac{\bar{\Phi}_s/\omega}{\bar{\Phi}_o} \tag{9}$$

where

$$\bar{\Phi}_s = \frac{\Phi_s}{F_s} = \frac{kS_s}{F_s} \tag{10}$$

and

$$\bar{\Phi}_o = \frac{\Phi_o}{F_o} = \frac{\Phi_s'}{\rho F_o} = \frac{kS_o}{\rho F_o} \tag{11}$$

Thus,

$$f_r(\theta_o;\theta_s,\phi_s) = \left(\frac{kS_s}{F_s\omega}\right)\left(\frac{\rho F_o}{kS_o}\right) = \left(\frac{S_s/F_s}{S_o}\right)\left(\frac{F_o\rho}{\omega}\right) \tag{12}$$

In most of the data reported, incidence was nearly normal, i.e., $\theta_o \approx 0$.

The azimuth angle of reflectance ϕ_S was always either 0 or π, that is, in the plane of incidence.

3.2 SYSTEM PARAMETERS FOR BRDF MEASUREMENT

For the system used in this work (Section 2.5) the telescope clear aperture was 0.87 in. in diameter and the telescope-to-mirror distance R was 31 in. Thus, ω was 6.2×10^{-4} sr. The reflectivity of the test mirror was 0.90 at 10.6 μm. The on-axis attenuation used in every case was the maximum attenuation 1.43×10^{-5}. Thus, the parameter $(F_o\rho/\omega)$ was 0.0208 for all data taken.

The detector signal on axis (specular beam) ranged from 30 mv at the start of the test to 18 mv at the conclusion. It is not known whether this degradation was due to deterioration of laser or detector performance, but signal levels did not change measurably during a day's operation. With all filters removed and a minimum measurable signal of 0.5 μv, the system dynamic range is approximately 3×10^9 with a minimum measurable BRDF of approximately 5×10^{-7}/sr.

It must be assumed that there is scattering from all system components, especially those prior to the 0.4-in.-diam chamber port entrance aperture. The radiation entering the chamber through the aperture must, therefore, be assumed to consist of the primary laser beam with accompanying divergent radiation several orders less intense. The purpose of using a spherical concave mirror was to image the entrance aperture on the telescope lens, thus eliminating specular reflection of scattered radiation for all telescope positions away from this image. In the actual case, the aperture was 63 in. from the mirror, mirror focal length was 25 in., and the telescope was 31 in. from the mirror.

The result is that the aperture focuses at 41.5 in. from the mirror and is not well focused at the telescope entrance. The image is approximately 0.75 in. in diameter at the telescope entrance. The specular radiation at the location of the telescope entrance may be considered a nearly focused laser surrounded by a fuzzy image of the aperture of approximately 0.75 in. in diameter. Thus, there will be some specular reflection of extraneous scattered radiation until the telescope has been moved 0.38 in. or 0.7 deg beyond the location where the focused laser no longer enters the telescope aperture.

The BRDF normally decreases very rapidly after the telescope moves away from the focused laser beam. In order to provide a meaningful reference for angular measurements, zero was defined in these experiments as the last telescope position providing full on-axis signal. Measurements were made at 1/6-deg intervals, and the normal signal change of 10^3 as the laser moved off the telescope lens gave an unambiguous zero.

As a result of the size of the lens, angle measurements in a region of rapidly changing BRDF (i.e., near specular) are in error by approximately the angle subtended by one-half the lens diameter (0.75 deg). This is because nearly all the energy received by the telescope is at the edge of the lens.

4.0 TEST PROCEDURES

4.1 PRELIMINARY EQUIPMENT TESTS

4.1.1 Filter Box Output Distribution

A check of the output energy distribution from the laser attenuator box was made to verify operation of the source unit. This test was

accomplished by using the telescope and swing arm with the pivot point located at the attenuator box exit aperture. Using procedures identical to a BRDF measurement, an "emittance distribution function" was obtained as a measure of the energy distribution in the filter box output. The results are presented in Fig. 7 where a decrease of five decades is seen for a 1-deg position change.

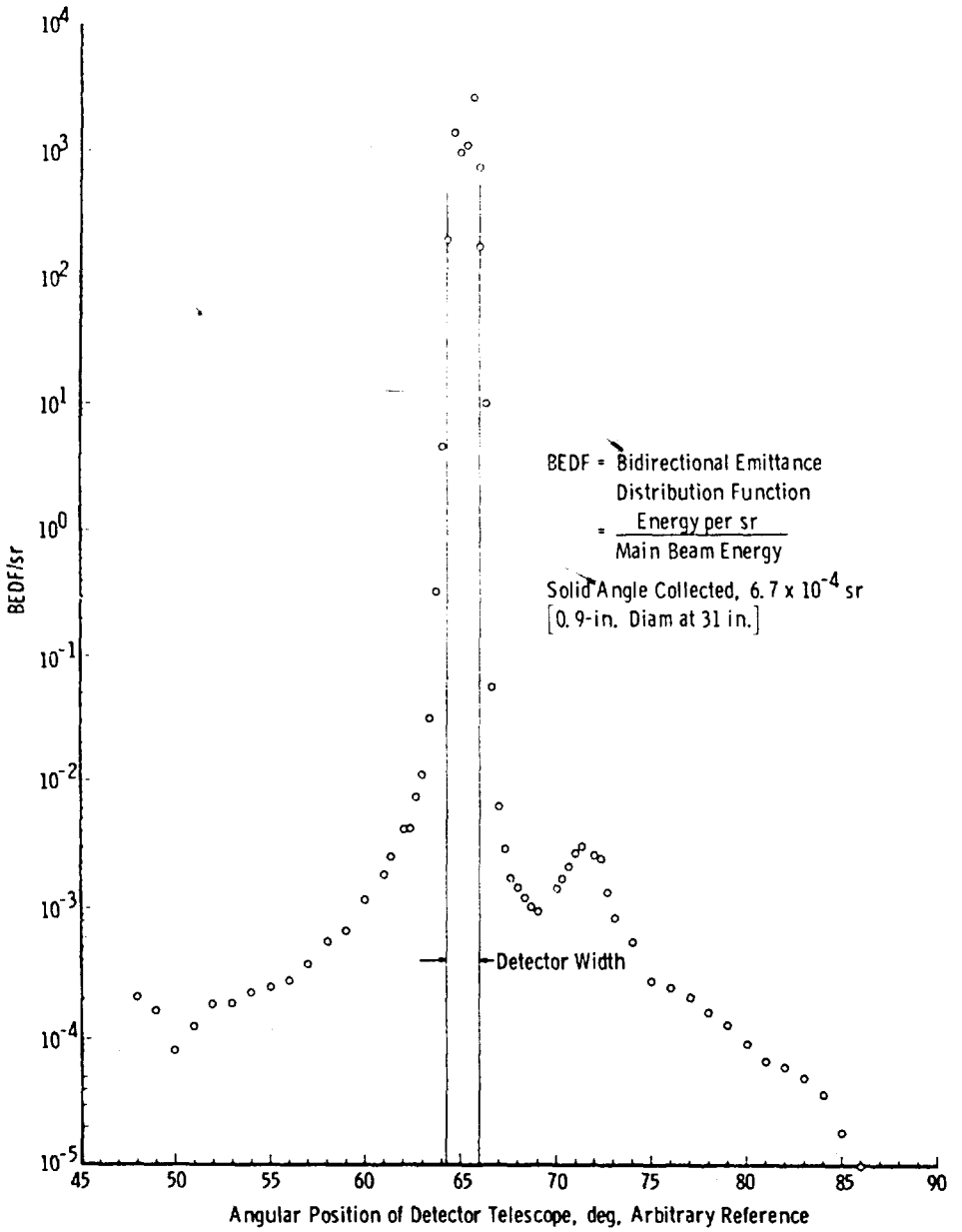

Figure 7. Laser filter box output distribution.

Additional elements used during the test introduced some additional scatter in the beam entering the chamber; however, the figure provides an indication of system capability in the region where the telescope views the field stop through the test mirror. The distribution function as shown represents the system limits of BRDF measurement for a large, flat, sample mirror viewed by a wide field of view detector. For the 25-in. focal length spherical test mirror, source scatter is limited to 0.7 deg on each side of the specular beam (see Section 3.2).

4.1.2 Telescope Focus and Field of View Measurements

It was necessary to focus the telescope for the 31-in. distance from the telescope lens to the test mirror. This was accomplished by using an incandescent Glo-Bar® source behind a 0.025-in. pinhole located 31 in. from the telescope lens. By traversing the source assembly and measuring detector output, the telescope field of view was mapped. Focusing was accomplished by adjusting the lens position for best on-axis sensitivity and out-of-field rejection. The results are shown in Fig. 8, where spot size is very close to the calculated value and out-of-field rejection is better than one decade for energy from the mirror more than ±1 cm (±0.7 deg) from the mirror center. It should be clear that a focused telescope offers a considerable advantage over a bare detector in terms of both optical gain and unwanted energy rejection.

A limitation of this procedure is that the radiation source used for focus was broadband with the germanium lens passing radiation above 1.8 μm. Since the index of refraction of the lens varies slightly with wavelength, there is a small focus error when the result above is used with the 10.6-μm laser source.

4.2 MIRROR SCATTER MEASUREMENT

A mirror scatter measurement was taken by rotating the test mirror to the position normal to the incoming laser beam. The entrance field was located slightly above the chamber centerline, and the telescope slightly below, so that the telescope passed under the beam without blockage. After verification of system alignment, a series of measurements was taken across the specular beam to obtain an on-axis signal measurement. Care was necessary with respect to filter position versus instrumentation position, since full laser power could destroy any detector used in this test. One pyroelectric detector and two thermopiles were cremated during the development of a satisfactory operating procedure.

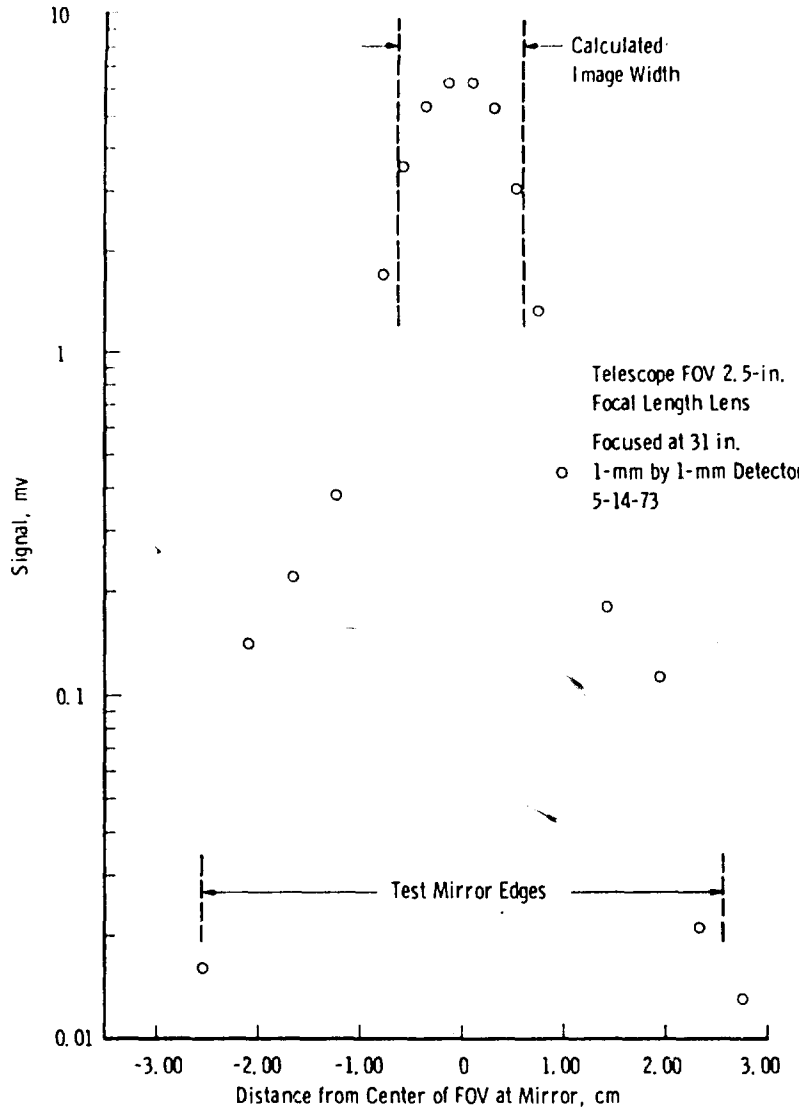

Figure 8. Telescope field of view.

Position increments of 1/6 deg were usually used (0.5 deg on a resolver geared 3:1 with respect to telescope arm). As the telescope moved out of the specular beam, increments of 1/6 deg or less were used and filters removed as necessary to maintain adequate signal level. As signal change became less rapid, larger increments of arm position were used. A sample set of data for a clean mirror measurement is shown in Table 1.

4.3 CRYODEPOSIT DEPOSITION

Cryodeposit depositions were made in the same manner as the previous work (Ref. 1). The measurement of rates and thinknesses was improved by use of the in situ thickness monitor (see Section 2.4), and improvements in the gas addition system improved mixture accuracy and ease of operation.

After the test mirror was cooled and in the deposition position, desired source pressure of the test gas was set in a reservoir connected to the U-tube. Since the reservoir was much larger than the U-tube and its supply line, valving in the U-tube to start flow did not appreciably affect the reservoir pressure. Makeup gas flow to the reservoir was then adjusted to maintain source pressure. Since the source pressures used were generally less than ambient, standard vacuum leak check procedures were used during assembly of the gas supply system.

For short deposition times, it was necessary to stop deposition quickly to ensure a uniform rate for the deposit. In these cases, the test mirror was rotated out of the gas flow as quickly as possible, simultaneously with shutoff of the gas flow. Gas trapped in the U-tube supply line was thus cryopumped in the chamber and did not contribute to the mirror cryodeposit.

For the gas mixture data, each gas was metered into a mixing chamber at ambient pressure and with a total flow rate much higher than the capacity of the U-tube. Excess gas was vented to atmosphere. The mixture was then used as the reservoir source for the procedure described in the previous paragraph.

Addition of water vapor to a dry gas mixture was more difficult. The mixing apparatus above was used to mix the dry gases in the desired proportion. This mixture was in turn mixed with water vapor at room temperature from a water reservoir, with flow maintained by a vacuum pump. The water vapor and dry gas mixture were independently metered into the mixing chamber and the mixture controlled by adjusting the supply of dry gas mixture. Available stagnation pressures were rather low, since the H_2O partial pressure in the system could not exceed the saturation pressure corresponding to the coolest element in the system. The source tube assembly in the chamber was maintained at temperatures approximately 10°F above ambient by a circulating water system supplying the source tube water jacket. In addition to

prevention of water vapor condensation in the source, the system also provides cooling for the source tube during heated gas operation.

4.4 RANGE OF TEST CONDITIONS

The range of cryodeposit conditions covered in this experiment is shown in Table 2. The mirror temperature range is limited at the low end by the GHe refrigeration supply temperature, while the upper limit is determined by the vapor pressure characteristics of the particular gas. The maximum gas stagnation temperature was limited by burnout of the platinum source tube for all gases except those containing NH_3, where the upper limit was the temperature at which dissociation was observed. This dissociation was detected by an increase in chamber pressure due to H_2 which cannot be cryopumped on a 20°K surface.

The BRDF measurements of cryodeposits were all made with the laser at near normal incidence to the test mirror. Test time did not allow measurement at other angles of incidence except for a few bare mirror runs near the end of the test.

With the exception of a small amount of random incident N_2 and O_2, all gas depositions were made with directed flow (molecular beam) at normal incidence to the mirror surface. This was believed to be the best simulation of the flight environment of a cryogenically cooled mirror, and test time did not provide for investigation of other deposition configurations.

4.5 FACTORS AFFECTING THE DATA

4.5.1 Telescope Ground

An electronic problem affected low signal level data for runs 0 through 37. High noise levels overloaded the lock-in amplifier pre-amp for signal levels less than 5 μv if the 5-μv full-scale gain setting was used. This was found to have been caused by anodizing the telescope barrel immediately prior to run 0 and was remedied by separately grounding the telescope.

4.5.2 Particle Contamination from Drive Screw

Particulate contamination was first noted after run 35 but was believed to be caused by cryodeposit deposition sequence. Increased

bare mirror scatter was observed during the next group of runs but was also attributed to deposition sequences and time in chamber. On removal after run 74, it was found that the telescope swing arm drive nut had become a particle generator aimed at the test mirror. Use of a teflon nut and shield and a mirror cleaning returned the test mirror to normal baseline operation which could then be maintained for long operating periods.

4.5.3 Change of Source Orifice

Depositions for all runs after run 151 were made using a 0.028-in.-diam orifice in the source U-tube rather than the original 0.013-in.-diam orifice. The change was made in order to obtain reasonable deposition rates with the low source pressures available for water vapor. This changed the relationship of source pressure to deposition rate but had no observable effect on results.

4.5.4 Reflections from Telescope Components

Inspection of Table 1 reveals two segments of angular position which have high apparent BRDF. These are at 2 deg and 4 deg, respectively, and were observed for all data. A post-test investigation revealed that these positions allowed edge reflections of the main laser beam from telescope mounting hardware to illuminate hardware surrounding the test mirror. Shielding this hardware with an absorptive surface produced a smooth BRDF curve for the bare mirror. In order to eliminate this effect, data at these angular positions have been deleted.

5.0 RESULTS AND DISCUSSION

5.1 BARE MIRROR DATA

There were 56 scatter measurements made on the bare test mirror (no cryodeposits) during the course of the test, and numerous measurements were made in the development of the measurement apparatus and adaptation of the unit to the vacuum chamber. Once the quality of the test mirror was established as a measurement baseline, it was necessary to make bare mirror measurements throughout the test to verify cleanliness of the test mirror. This was especially important since the chamber was not located in a clean room, and there was a period of likely contamination between the time the mirror cover was removed

and the completion of chamber closure and pumpdown. Provisions had been made for a portable clean booth to be mounted over the chamber, but it was experimentally determined that if the chamber was immediately closed and pumped after cover removal the clean booth was not necessary to maintain cleanliness within the current ability to measure BRDF. A study of effects of atmospheric contamination is reported in Ref. 8.

A complete tabulation of all bare mirror scatter data is presented in Table 3. Runs which did not represent a clean mirror are so noted and include runs 0 through 36 and 42A through 73 (see Sections 4.5.1 and 4.5.2). These data are included in Table 3 for use in comparing with cryodeposit data run under the same conditions.

A mean and standard deviation for the remaining data is tabulated at the end of Table 3. These data are plotted in Figs. 9 and 10, and a least squares curve fit is also shown. Runs designated with an asterisk in Table 3 were not used in calculating the mean and curve fit.

5.2 NITROGEN–DIRECTED INCIDENCE

Scatter data from nitrogen cryodeposits formed by the molecular beam are presented in Table 4. Run 120 is of considerable interest, as it was highly visible but showed no increase in infrared scatter. Figure 5, used to show the test section installation, was taken with the cryodeposit of run 120 on the mirror. It should be clear why early attempts during this work to correlate cryodeposit visibility with scatter at 10.6 μm were quickly revised. It was, in general, possible to obtain a visible, frosty appearing, N_2 deposit by depositing at a mirror temperature only slightly less than the maximum condensation temperature. No IR scatter was found with such deposits. Deposits made at lower mirror temperatures showed neither visible nor IR scatter.

It was possible to obtain IR scatter from an N_2 deposit by slowly warming the mirror until partial vaporization occurred as is shown in Fig. 11. Run 147 shows that removal of approximately one-half of the cryodeposit of 146 increased IR scatter by approximately two decades. An additional two decades of IR scatter were obtained by adding a cryodeposit to the partially purged one of run 147. This is shown for run 148, which has four decades higher scatter than a clean mirror.

5.3 OXYGEN–DIRECTED INCIDENCE

Oxygen was the only gas which caused a consistent increase in scatter with deposited thickness. The data are shown in Table 5.

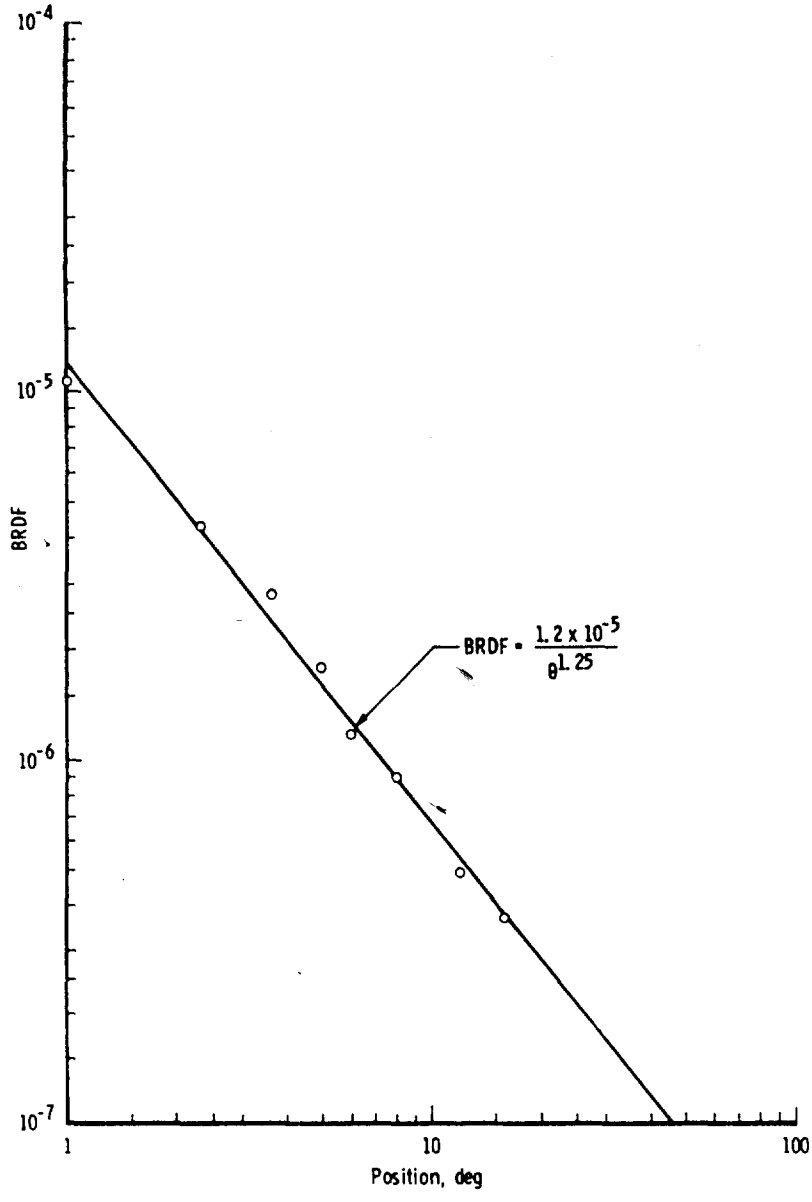

Figure 9. Clean mirror baseline, logarithmic.

Because of the particle contamination problem (see Section 4.5.2), most of the depositions of runs 40 through 74 were repeated, as it appeared the contamination might have been responsible for all the observed scatter. The repeat data verified the earlier data. In general, all oxygen cryodeposits were visible with a frosty appearance and showed increased IR scatter.

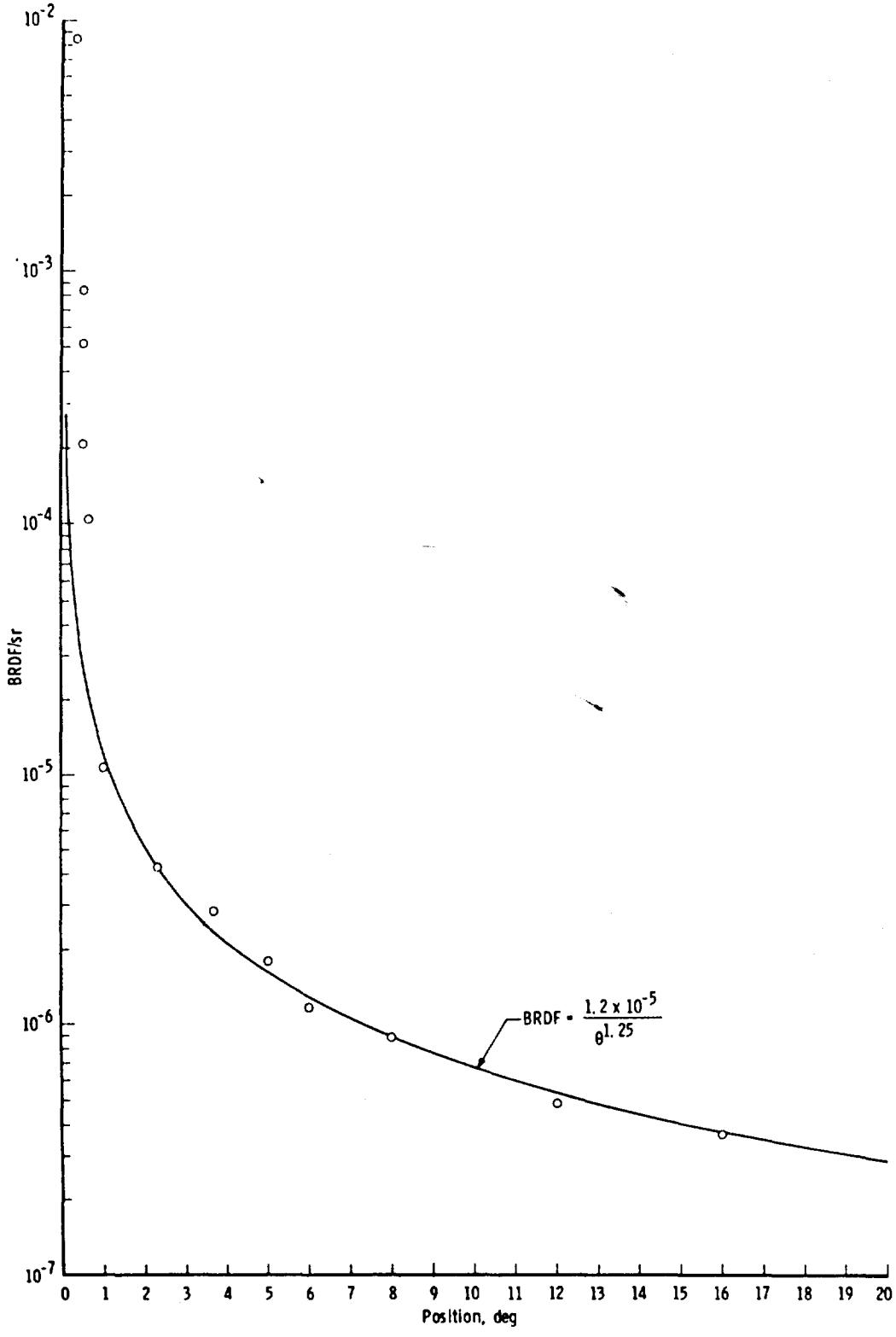

Figure 10. Clean mirror baseline, semilogarithmic.

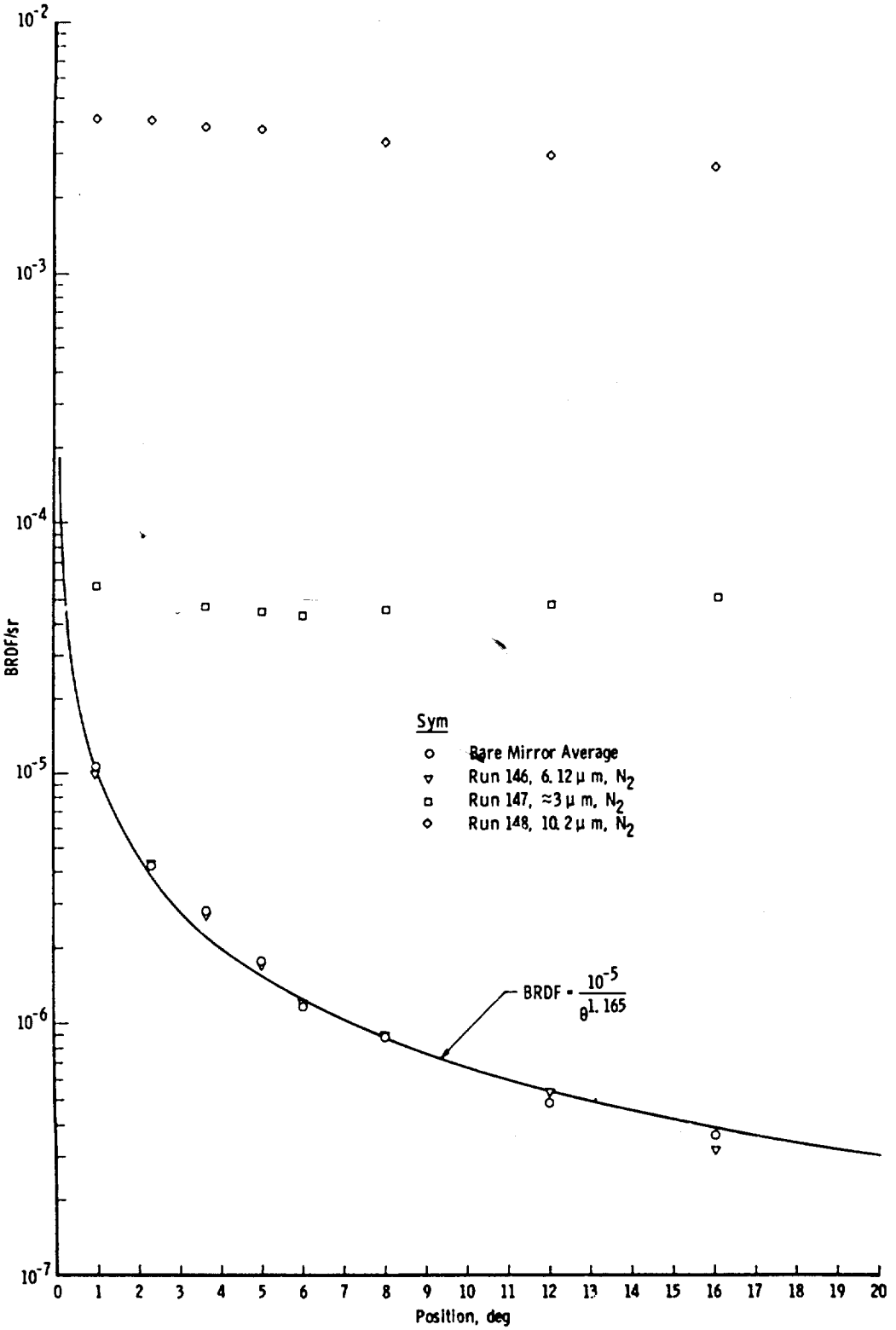

Figure 11. Effects of partial vaporization, N_2.

Figure 12 shows the increase in scatter with thickness for a sequence of cumulative deposits of 300°K gas on a 22°K mirror. The

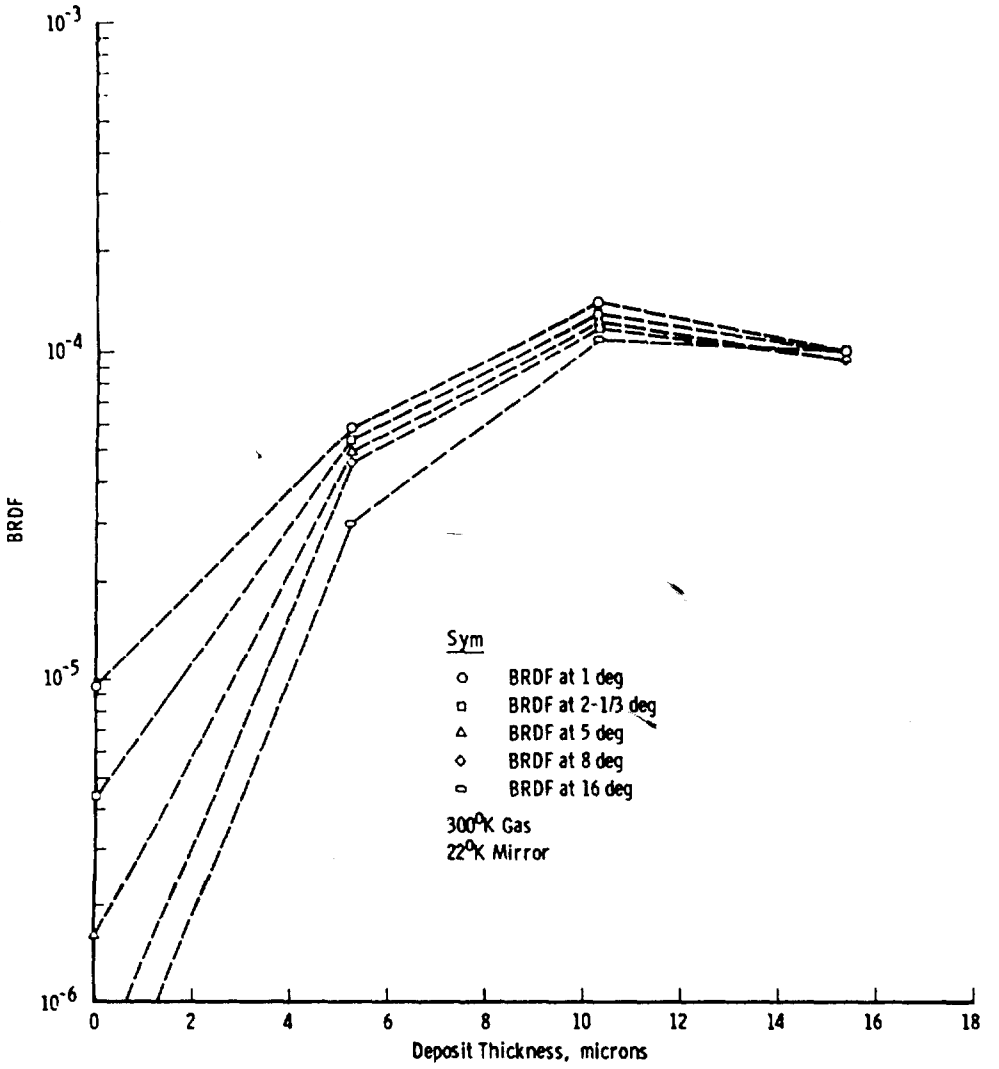

Figure 12. O_2 runs 75 through 78.

maximum scatter at 10 μm was also observed in the series of deposits with 1000°K gas on a 26°K surface as shown in Fig. 13. Figures 14 and 15 present earlier data which correspond to the trend of Figs. 12 and 13, although contamination effects are evident. The zero thickness measurement is the starting bare mirror condition, and in Figs. 14 and 15 the bare mirror measurement at the end of the sequence is shown for reference.

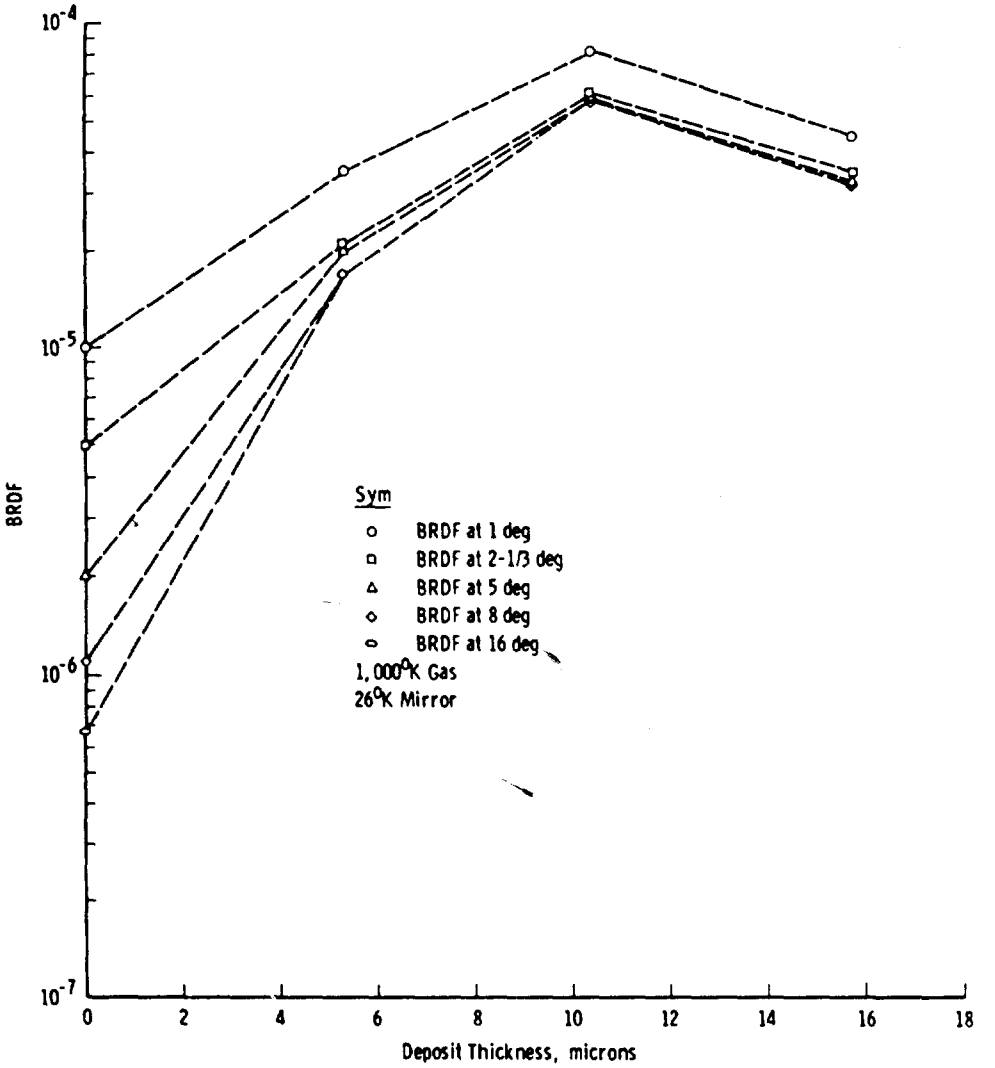

Figure 13. O_2 runs 166 through 169.

The observed maximum at 10-μm thickness and the trend toward another at 20 μm in Fig. 15 suggest an interference effect on the scatter measurements at thickness multiples of the 10.6-μm CO_2 laser source.

5.4 CARBON DIOXIDE–DIRECTED INCIDENCE

Carbon dioxide caused increased IR scatter if deposited on a low temperature surface (20 to 25°K) but not when deposited at near maximum mirror temperature of 80°K, as is shown in the data of Table 6.

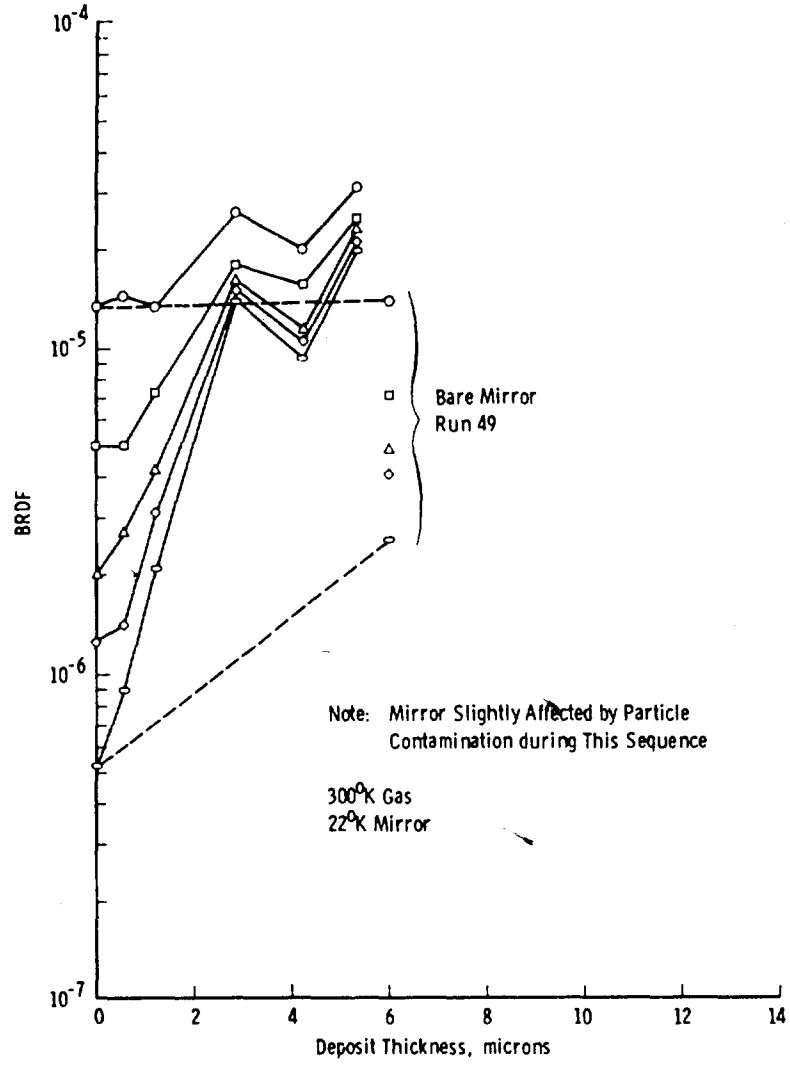

Figure 14. O_2 runs 42A through 49.

Runs 101 and 102 at high mirror temperature show no IR scatter, while all data at low mirror temperature and greater than 5-μm thickness showed increased scatter. Figures 16, 17, and 18 show the data for the three cumulative deposits at low temperature. Increased IR scatter appears first at large angles then shows a general increase as the deposit thickens.

Although the trends are the same for the three sets of data, there is no repeatability for a given thickness. One partial explanation is that the mirror temperature for runs 83 through 86 was 26°K while runs 91 through 99 were on a 21°K mirror. This does not explain the difference between runs 93 and 95. It should be noted that although the total

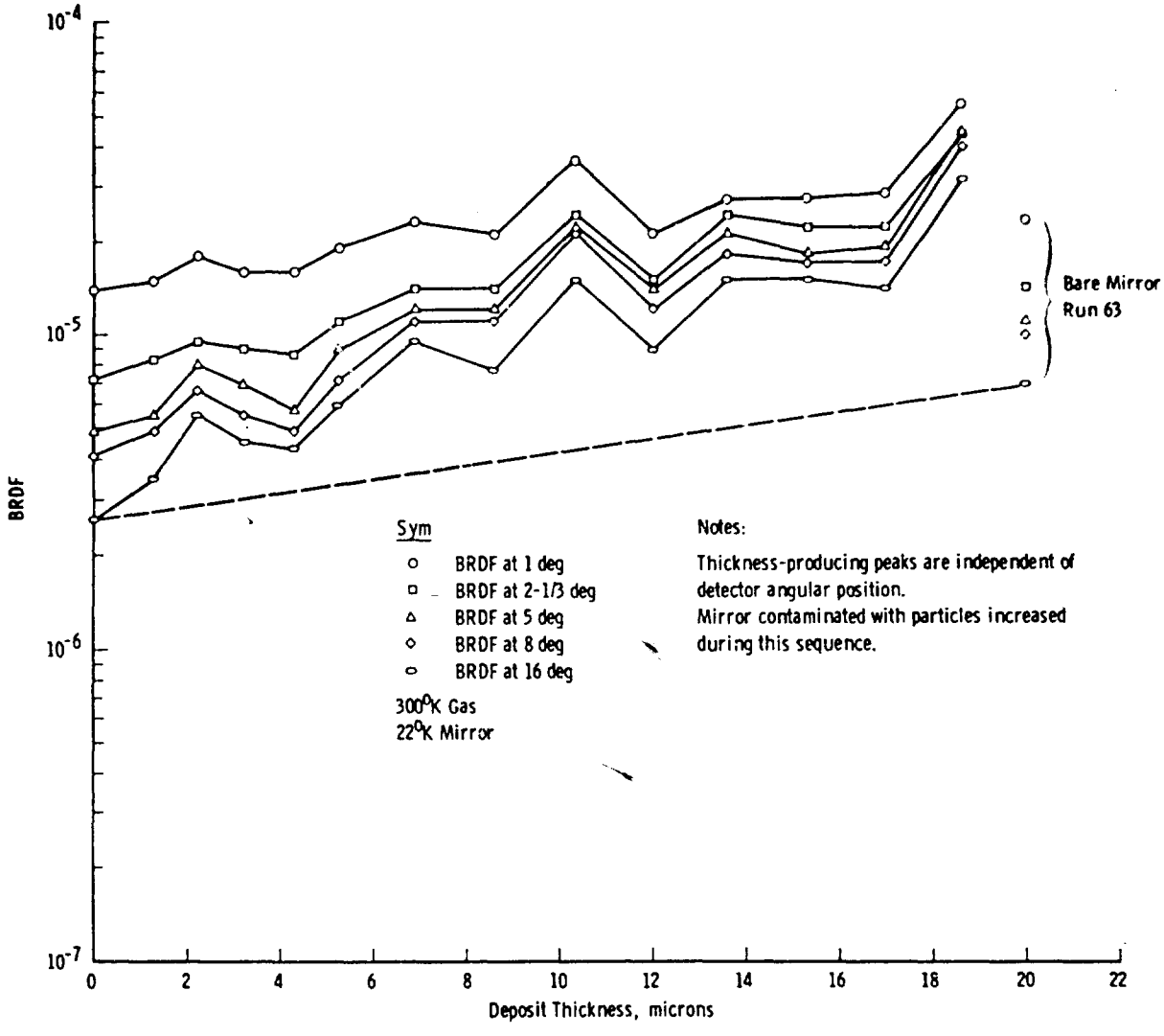

Figure 15. O_2 runs 49 through 63.

thickness is similar for these runs, the deposition was discontinuous for run 93, and deposition transients or time between deposits may be significant. This possibility was not investigated.

The series of runs 86 through 89 is of particular interest. Part of the cryodeposit of run 86 was removed by rotating the mirror back into deposition position, then slowly warming the mirror while observing the thickness monitor. In this manner a known portion of a cryodeposit could be removed, and vaporization stopped at the desired thickness. Considerable care was required in control of mirror temperature for this operation. The data for run 87 show that partial removal resulted

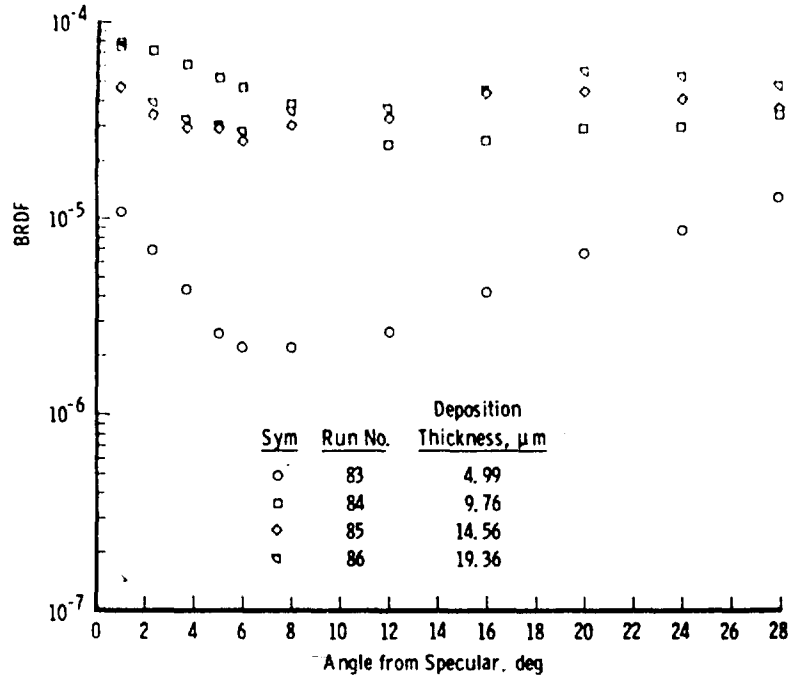

Figure 16. CO_2 runs 83 through 86.

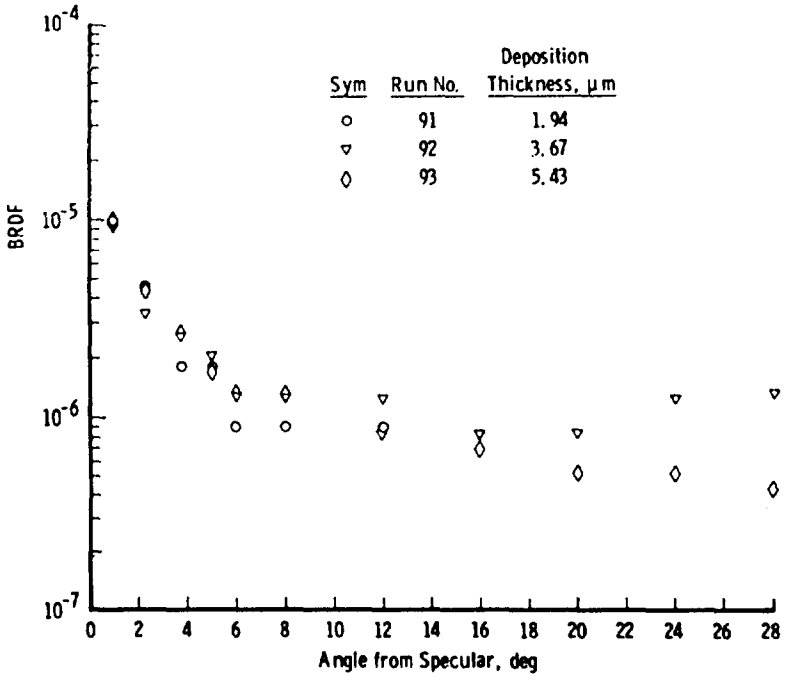

Figure 17. CO_2 runs 91 through 93.

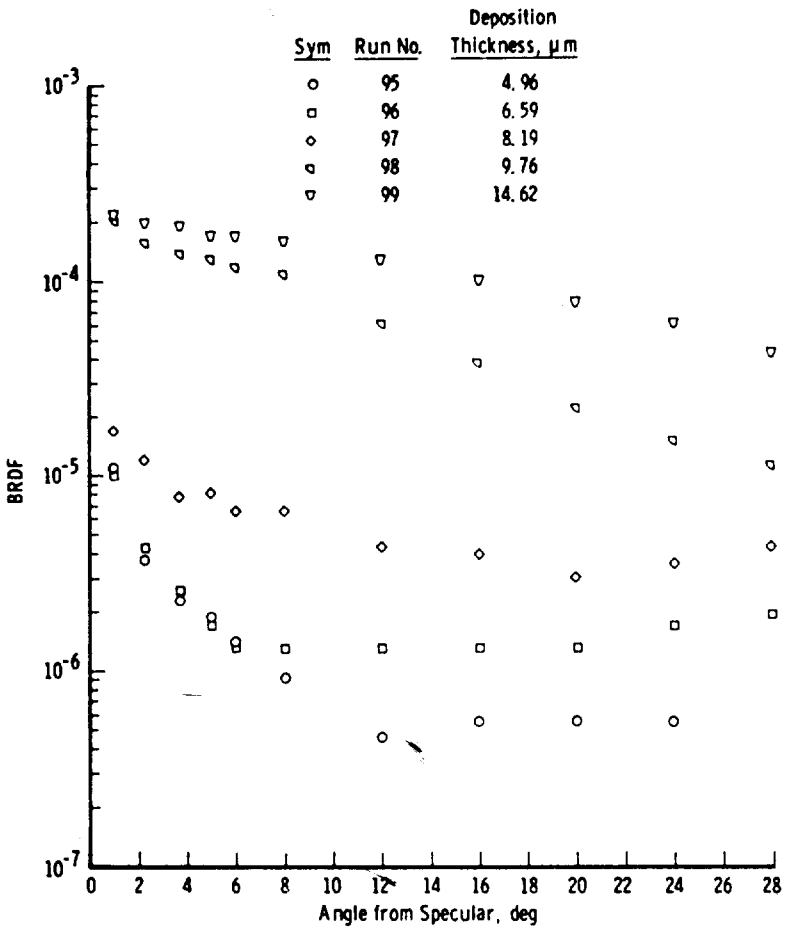

Figure 18. CO_2 runs 95 through 99.

in a three-decade increase in mirror scatter. Following run 87, the mirror was warmed to 108°K until all the CO_2 had evaporated. However, visual inspection revealed that a slight film remained on the mirror. Run 88 shows that some degradation existed relative to a clean mirror but less than a decade. A deposit was then made for run 89, but visual scatter rendered the thickness monitor useless, and the deposit was estimated from time and source pressure. Scatter for the new deposit of 5 μm was slightly higher than run 87 and degraded more than four decades from a clean mirror.

The final observation is run 103. As previously noted, no scatter resulted from the 10-μm deposit on a 73 to 80°K mirror. However, when the deposit of run 102 was cooled, it shattered at approximately 60°K. The result was a series of hairlike crystals radially outward

from the center with large areas of the mirror clean. The outeredge of the deposit was apparently intact but appeared diffuse white. IR scatter for the resulting crystals on the mirror was approximately five decades greater than a clean mirror.

5.5 AMMONIA–DIRECTED INCIDENCE

5.5.1 IR Scatter Data

Of all gases tested, ammonia was most unpredictable because of its tendency to shatter or crystallize, either during deposition or if mirror temperature is changed after deposition. The data are presented in Table 7. Only runs 108, 152, and 153 show no significant scatter. Run 108 did show visible evidence of beginning crystallization or shatter and can be seen in Fig. 19. However, additional cryodeposit caused an increase of six decades in BRDF and resulted in very

Figure 19. Cryodeposit, run 108.

crystalline appearing cryodeposits. These cryodeposits are shown in Figs. 20 and 21. Runs 152 and 153 showed no increased scatter for thicknesses up to 10 μm. This condition (hot gas, cold mirror) resulted in a nearly invisible cryodeposit. After measurement, this cryodeposit was slowly heated, and at 60°K the cryodeposit suddenly changed to a diffuse white with an attendant rise in scatter of five decades as shown by run 154.

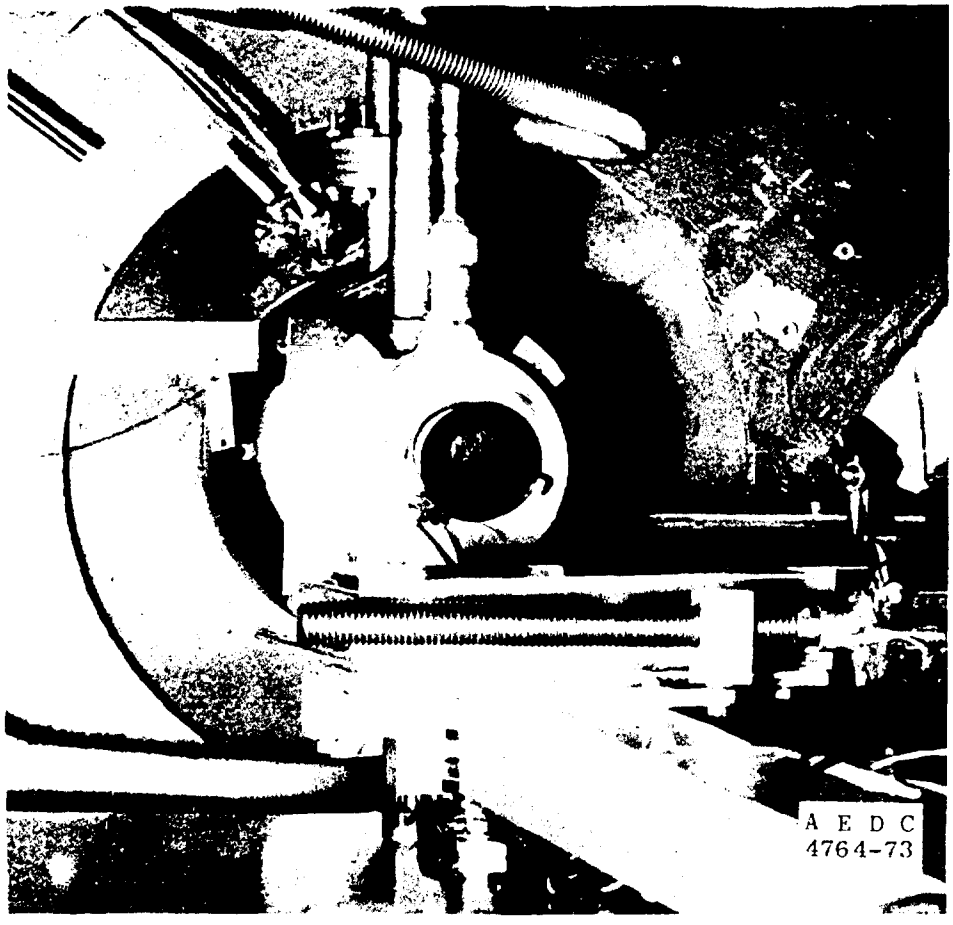

Figure 20. Cryodeposit, run 109.

Runs 112, 114, and 115 all exhibited a slight increase in scatter. Run 112 was made on a 77°K mirror (near maximum) and runs 114 and 115 at 51°K. These cryodeposits were unusual in that they did not shatter during warmup to vaporization, although a frosty appearance was observed at vaporization. No attempts were made to cool these cryodeposits after the scatter measurements.

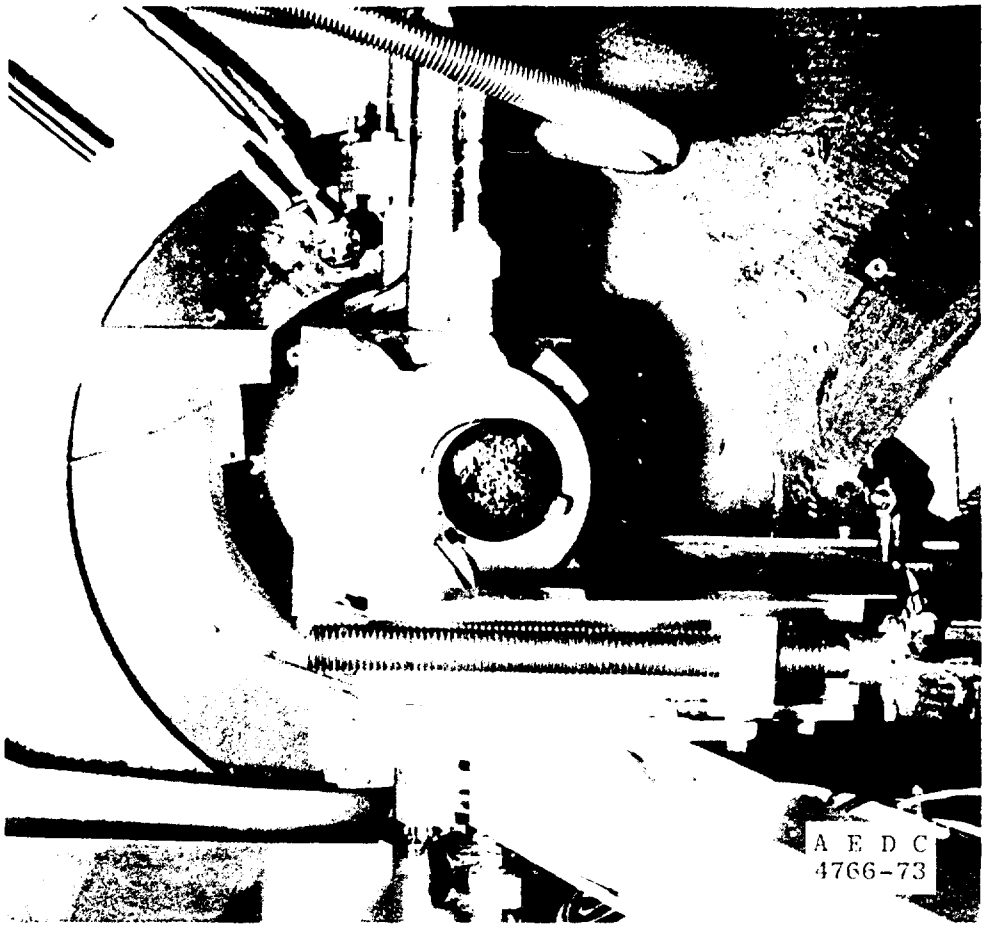

Figure 21. Cryodeposit, run 110.

Runs 155 and 156 (hot gas, maximum mirror temperature) also exhibited some scatter increase but did not crystallize during deposition. However, when the deposit cooled to 46°K it shattered and the majority fell off the mirror. The few crystals remaining account for the four-decade increase in scatter shown in run 157.

All remaining runs were very crystalline with corresponding high IR scatter. In some cases the crystalline pattern grew with the deposit as in Figs. 19 thru 21. In other cases, however, the change occurred instantaneously as evidenced by abrupt signal level changes in the thickness monitor detectors. A majority of these abrupt crystallizations occurred at a thickness of about 2 μm.

5.5.2 Persistence of Crystal Patterns

A phenomenon associated with fracturing or crystallization was observed which raises the possibility of gaseous contamination effects.

With most gases, and with those ammonia cryodeposits which evaporated smoothly, no visible or IR effects were observed after the vaporization temperature for the species was passed. However, if fracturing occurred, a pattern of the remaining crystals remained visible on the mirror until the mirror was well above room temperature.

Water vapor does not offer an adequate explanation, as water cryodeposits (discussed later) evaporated by the time the mirror attained a temperature of about -100°F during warmup under vacuum. It was experimentally found that heating the mirror to 130°F to 150°F was necessary to ensure removal of all traces of cryodeposits.

5.5.3 Index of Refraction Data--Ammonia

As a part of the thickness measurement for each cryodeposit, index of refraction was calculated and is shown on all data sheets. As was previously reported in Ref. 1, ammonia exhibits large differences in index of refraction dependent on deposition conditions. The current work also shows these variations and is apparently due to different cryodeposit structure. This may be related to the sudden fracturing or crystallization observed during temperature changes of a cryodeposit, although it does not seem consistent with fracturing during deposition.

5.6 CARBON MONOXIDE, WATER VAPOR, AND AIR-DIRECTED INCIDENCE

5.6.1 Carbon Monoxide

Runs 126, 128, and 130 were taken on carbon monoxide cryodeposits and are shown in Table 8. No significant increase in IR scatter was found for conditions used. No hot gas runs were made, but the full range of available test mirror temperatures for this gas was covered.

5.6.2 Water Vapor

Five runs (Table 8) were made with water vapor cryodeposits at mirror temperatures ranging from 27°K to 74°K. The deposit of cold gas on a cold mirror shattered during deposition, similar to NH_3, with accompanying IR scatter as shown by run 159. Run 160 was cold gas on a warm mirror (74°K) and showed no IR scatter. This cryodeposit was subsequently cooled to 32°K then warmed to vaporization without significant visible changes. Run 163 (37°K mirror) was identical to Run 160, while the deposit of run 161 (hot gas, cold mirror) shattered during slow

warmup at 120°K, with IR scatter of the shattered cryodeposit shown as run 162, up five decades.

It should be noted that water absorbs 10.6-μm radiation, and this effect shows up in the reduced BRDF for nonscattering cryodeposits. In order to be consistent with the definition of BRDF, the greatly reduced on-axis detector signal was not used in calculating BRDF; rather, the signal on a bare mirror run during this time period was used as the best indication of incident power.

5.6.3 Ambient Air

Five runs were made using ambient air as the test gas; these are shown in Table 8. None of these deposits showed any increased IR scatter. Runs 133 and 135 were made at mirror temperatures which would not cryopump all constituents. Run 134 eliminated N_2, while run 133 eliminated both N_2 and O_2 and was therefore a very thin cryodeposit, not measurable with the thickness monitor (< 1 μm).

Run 136 was made by admitting air in spurts directly into the test chamber with the mirror facing the inlet and is therefore not quantitative.

5.7 MIXTURES–DIRECTED INCIDENCE

5.7.1 Ammonia–Nitrogen

Of the seven NH_3-N_2 cryodeposits measured (Table 9), there was no large increase in IR scatter unless the deposit shattered. It should be recognized that the mirror temperature determines whether one or both of the constituents is deposited on the test mirror. Run 139 is anomalous in that a slight increase in IR scatter was measured (factor of five) without any visual evidence of scatter.

Shattering occurred under two conditions. If both components had been deposited at a mirror temperature of less than 30°K, the deposit would have shattered on warmup as the nitrogen vaporized (runs 140 and 144). Run 142 was deposited at 35°K; thus, only NH_3 was deposited. This deposit shattered during deposition. Thicknesses and indices of refraction for all mixture deposits are based on the gas actually deposited.

5.7.2 Simulated Propellant Gas

Six runs were made using a mixture intended to simulate a bipropellant engine exhaust (Table 9). The mixture was composed of 3.2-percent CO, 11.3-percent CO_2, 39.0-percent N_2, and 46.5-percent H_2O. Increased IR scatter was observed only if the cryodeposit shattered, and none of the deposits shattered during deposition. However, both cold mirror runs (170 and 174) shattered during warmup at 41°K and 42°K, respectively, with accompanying scatter increase of five decades.

5.8 NITROGEN AND OXYGEN–RANDOM INCIDENCE

During the early stages of the test, a number of runs were made using nondirected gas incidence. These are shown in Table 10 and include nitrogen data and some oxygen data. These data were all taken with increased detector noise levels (see Section 4.5.1), but since scatter levels were well above clean mirror data, these data are not affected.

The method of deposition was to leave the mirror in the normal deposition position so the thickness monitor could be used and to admit gas through a valve in the test section behind the test mirror. This arrangement resulted in a source best described as pseudo-random since the gas must bounce off surfaces which may be either 300°K or 77°K before arriving at the mirror surface. Because of the uncontrolled nature of these runs, little comment can be made except that the results indicate that randomly incident gas produces cryodeposits which scatter more than directed incidence. No shattering was observed, and only runs 16 and 25 exhibited extremely large IR scatter. Test section pressure during deposition is shown in Table 10.

6.0 SUMMARY OF RESULTS

6.1 BARE MIRROR DATA

Scatter measurements of the test mirror without cryodeposits showed that the mirror could be installed, uncovered, and the chamber closed and pumped down without special clean room precautions while maintaining an acceptable level of cleanliness. Further, the mirror

could be cycled through many cryodeposits without affecting mirror performance provided each set of cryodeposits was purged by warming to 130°F. The 130°F value was found experimentally, and no attempt was made to measure the effectiveness of lower temperatures for longer times.

Particulate contamination generated by a worn drive nut quickly deteriorated mirror performance. Further, a seeding action was noted as cryodeposits on a contaminated test mirror showed a disproportionate increase in scatter. The effects of contamination were even worse if the contamination occurred from an incompletely purged, previous cryodeposit.

6.2 SCATTER FROM WELL-BEHAVED CRYODEPOSITS

For cryodeposits which showed consistent deposition characteristics and did not shatter, only O_2 and CO_2 resulted in substantial increases in IR scatter. Both gases showed increases of up to two decades for cryodeposits of 10 to 20-μm thickness. For other gases, no increased scatter from the deposits was measured. Partial vaporization of most cryodeposits caused increased scatter.

6.3 CORRELATION OF VISUAL APPEARANCE WITH IR SCATTER

There is no correlation between visible scatter and IR scatter if surface roughness is not accounted for. Many cryodeposits which appeared frosty white (high visible scatter) showed no measurable increase in IR scatter (for example, run 120, Fig. 5). Others which showed only a small number of crystals remaining on the mirror (low visual scatter) proved to be degraded by five or more decades in the IR. It is not surprising that a highly visible cryodeposit with very uniform small surface roughness does not scatter in the IR. It is surprising, however, that a cryodeposit of such characteristics can be formed.

Visual inspection of the test mirror came to rely primarily on a search for particles or crystals on the surface, and this was best done using a He-Ne laser with chamber and room lighting turned off.

6.4 SHATTERING OF CRYODEPOSITS

By far the most catastropic possibility in terms of mirror performance is that of a cryodeposit shattering. This phenomenon was

observed under certain conditions with ammonia, carbon dioxide, and water vapor. Some deposits shattered during deposition; others shattered when a stable, nonscattering cryodeposit was warmed or cooled. Increases in IR scatter of five to six decades were common. Some evidence was found that phase changes were involved, but this investigation was not sufficiently adequate to clearly define the causes and prevention of this occurrence.

An experimental observation throughout the test was that if mirror warmup was started, it was necessary to complete the warmup to above room temperature in order to completely clean up the mirror. Further, if shattering occurred, an outline of the resulting crystal pattern persisted to mirror temperatures well above those required to vaporize any of the test gases. If a cryodeposit was put on with a shadow of a preceding shattered cryodeposit remaining on the mirror, the new cryodeposit tended to assume the original pattern. In such cases, IR scatter was much larger than for a deposit on a clean mirror even though IR scatter of the mirror prior to the deposit showed performance equal to a clean mirror.

6.5 EFFECTS OF MIXTURES

If single components were cryodeposited from mixtures, the cryodeposits exhibited the characteristics of that component, including the tendency to shatter. However, if the entire mixture was cryodeposited, no shattering was observed during deposition. On warmup, shatter occurred only as one component evaporated. It should be noted that these observations are based on a limited range of mixtures and deposition conditions, primarily N_2-NH_2.

6.6 REQUIREMENTS FOR CLEANUP

Removal of cryodeposits by vaporization under vacuum was accomplished successfully many times during the course of this investigation. However, it was found necessary to warm the test mirror to temperatures considerably greater than would be expected from the vapor pressure characteristics of the test gases. Further, if shattering occurred, the resulting pattern persisted long after the test gas had apparently vaporized. While this effect may be due to trace contaminants, there is no reason to believe that optical surfaces in use will see only pure gases. In general, it was found necessary to heat the test mirror to 130°F to ensure complete cleanup.

Use of IR scatter measurements was not sufficient to indicate return of the test mirror to its clean state. Low IR scatter measurements could sometimes be obtained while a barely visible trace of a previous cryodeposit remained. Deposition of a new cryodeposit would then show greatly increased scatter over a similar cryodeposit on a mirror previously heated to 130°F.

REFERENCES

1. Arnold, F., Sanderson, R. B., Mantz, A. W., et al. "Infrared Spectral Reflectance of Plume Species on Cooled Low Scatter Mirrors." AFRPL-TR-73-52 (AD777285), September 1973.
2. Thompson, S. B., Arnold, F., and Sanderson, R. B. "Optical Effects of Cryodeposits on Low Scatter Mirrors." AIAA Paper No. 73-732, presented at AIAA 8th Thermophysics Conference, Palm Springs, California, July 16-18, 1973.
3. Heald, J. H., Jr. and Brown, R. F. "Measurements of Condensation and Evaporation of Carbon Dioxide, Nitrogen, and Argon at Cryogenic Temperatures Using a Molecular Beam." AEDC-TR-68-110 (AD674596), September 1968.
4. Arnold, F., Busby, M. R., and Dawbarn, R. "Experimental Investigation of the Scattering of a Nitrogen Aerodynamic Molecular Beam from a Solid Nitrogen Surface." AEDC-TR-70-172 (AD712374), October 1970.
5. Dawbarn, R., Arnold, F., Stephenson, W. B., et al. "Development of an Integrated Cryogenic Pumping System for Rocket Plume Studies." AEDC-TR-71-19 (AD880649), February 1971.
6. Scheele, S. R. "Scattering Characteristics of Mirrors and the Associated Inverse Scattering Problem." Report Reference M73-82, Hughes Aircraft Company, Electro-Optical Division, Culver City, California, November 1973.
7. Tempelmeyer, K. E., Wood, B. E., and Mills, D. W., Jr. "In Situ Measurement of Thickness and Other Properties of Carbon Dioxide Cryodeposits by Optical Techniques." AEDC-TR-67-226 (AD662869), December 1967.
8. Young, R. P. "Degradation of Low Scatter Mirrors by Particle Contamination." AEDC-TR-74-109 (AD-A004103), January 1975.

Table 1. Scatter Measurement, Raw Data Sample

Position Readout, deg	Signal, S_S, mv	Filters	Attenuation, F_S	Position, θ, deg	BRDF/sr
173.2	0.200	1 + 2 + 3	1.43×10^{-5}		
173.1	6.8	↓	↓		
173.0	21.0				
172.5	24.0				
172.0	25.5				
170.0	25.5				
169.0	25.0				
168.6	23.5				
168.5	8.5			0	
168.4	0.50				
168.3	0.060				
168.2	0.046				
168.1	0.022				
168.0	0.0135	↓	↓	0.17	
167.5	0.092	1 + 2	2.16×10^{-3}	0.33	3.48×10^{-2}
167.0	0.640	None	1.0	0.5	5.22×10^{-4}
166.5	0.080	↓	↓	0.67	6.52×10^{-5}
166.0	0.015			0.83	1.22×10^{-5}
165.5	0.0092			1.00	7.50×10^{-6}
164.5	0.0075			1.33	6.12×10^{-6}
163.5	0.0068			1.67	5.55×10^{-6}
163.0	0.023			1.83	1.88×10^{-5}
162.5	0.014			2.00	1.14×10^{-5}
162.0	0.0055			2.17	4.49×10^{-6}
161.5	0.0055			2.33	4.49×10^{-6}
160.5	0.0052			2.67	4.24×10^{-6}
159.5	0.0050	↓	↓	3.00	4.08×10^{-6}
158.5	0.0033	None	1.0	3.33	2.96×10^{-6}
157.5	0.0030	↓	↓	3.67	2.45×10^{-6}
157.0	0.007			3.83	5.71×10^{-6}
156.5	0.011			4.00	8.97×10^{-6}
156.0	0.007			4.17	5.71×10^{-6}
155.5	0.0028			4.33	2.28×10^{-6}
154.5	0.0028			4.67	2.28×10^{-6}
153.5	0.0022			5.00	1.79×10^{-6}
150.5	0.0015			6.00	1.22×10^{-6}
144.5	0.0011			8.00	8.97×10^{-7}
132.5	0.0007			12.00	5.71×10^{-7}
120.5	0.0005			16.00	4.08×10^{-7}
108.5	0.0003	↓	↓	20.00	2.45×10^{-7}

$$BRDF = \frac{S_S/F_S}{S_O} \quad \frac{F_O\rho}{\omega} = 0.0208 \frac{S_S/F_S}{S_O}$$

$S_O = 25.0$ mv

$$BRDF = 8.16 \times 10^{-4} \frac{S_S,}{F_S}$$

Table 2. Range of Test Conditions

Species	Mirror Temperature, °K	Gas Temperature, °K	Gas Stagnation Pressure, torr	Deposition Rate, μm/min	Deposition Thickness, μm	No. of Measurements
N_2	16 to 30	300 and 1,000	100 to 650	0.37 to 0.48	1.43 to 28.87	14
O_2	20 to 33	300 and 1,000	50 to 250	0.067 to 0.348	0.54 to 18.64	39
CO_2	20 to 80	300	250	0.26 to 0.35	1.94 to 19.36	17
NH_3	21 to 77	300 and 1,000	50 to 250	0.08 to 0.80	1.93 to 9.57	17
CO	21 to 31	300	50 to 250	0.08 to 0.37	5.50 to 5.79	3
H_2O	27 to 74	300 and 1,000	20	0.065 to 0.10	3.13 to 4.81	5
Air	21 to 39	300	50 to 250	0.038 to 0.38	1.83 to 6.34	5
60% N_2 40% NH_3	23 to 49	300	250	0.086 to 0.38	2.59 to 5.96	2
55% N_2 45% NH_3	21 to 39	300	250	0.13 to 0.35	1.59 to 5.95	3
33% N_2 67% NH_3	21 to 27	300	250	0.29 to 0.31	5.86 to 11.87	2
Plume Gas	24 to 52	300 and 1,000	5.4 to 6.5	0.04 to 0.10	5.04 to 5.51	6
N_2 (Random)	19 to 26	<300	1 atm	0.22 to 1.97	9.89 to 24.48	14
O_2 (Random)	21 to 33	<300	1 atm	0.077 to 0.60	1.42 to 11.15	3
Bare Mirror	20 to 300	---	---	---	---	>53

Table 3. Bare Mirror Scatter Measurements

Run No.	Source		Scatter								Remarks
			Position, deg								
	Chamber Pressure, torr	Mirror Temperature, °K	1	2-1/3	3-2/3	5	6	8	12	16	
			BRDF/sr								
0*	atm	300	8.9×10^{-6}	3.7×10^{-6}	2.97×10^{-6}	1.48×10^{-6}	1.48×10^{-6}	---	---	---	
1*	1.5×10^{-6}	21	1.53×10^{-5}	---	---	2.12×10^{-6}	---	2.54×10^{-7}	---	---	
2*	2.0×10^{-6}	333	7.64×10^{-6}	5.09×10^{-6}	2.55×10^{-6}	2.55×10^{-6}	1.7×10^{-6}	6.79×10^{-7}	---	---	
3*	atm	300	8.47×10^{-6}	---	---	1.16×10^{-6}	---	1.93×10^{-7}	---	---	
4*	1.0×10^{-6}	316	9.1×10^{-6}	5.2×10^{-6}	2.77×10^{-6}	1.99×10^{-6}	8.7×10^{-7}	6.07×10^{-7}	---	---	Runs 0 thru 36 affected by detector noise at low signal levels
5*	5.5×10^{-7}	24	1.68×10^{-5}	---	---	1.5×10^{-6}	---	2.5×10^{-7}	---	---	
6*	4.8×10^{-7}	20	1.75×10^{-5}	4.91×10^{-6}	2.33×10^{-6}	1.33×10^{-6}	9.1×10^{-7}	5.8×10^{-7}	---	---	
7*	5.0×10^{-7}	341	1.46×10^{-5}	---	---	---	---	---	---	---	
12*	7.8×10^{-7}	21	1.16×10^{-5}	---	---	1.54×10^{-6}	---	3.85×10^{-7}	---	---	
21*	8.0×10^{-7}	23	1.02×10^{-5}	---	---	1.61×10^{-6}	---	---	---	---	
31*	8.0×10^{-6}	23	2.65×10^{-5}	---	---	2.68×10^{-6}	---	7.56×10^{-7}	---	---	Contaminated - unknown cryo-deposit
35*	6.0×10^{-7}	24	2.64×10^{-4}	---	---	1.28×10^{-4}	---	4.64×10^{-5}	---	1.76×10^{-5}	Contaminated - unknown cryo-deposit
36*	7.0×10^{-7}	300	1.66×10^{-5}	---	---	7.07×10^{-6}	---	5.0×10^{-6}	---	3.08×10^{-6}	Contaminated - particulate
38	2.4×10^{-7}	316	1.08×10^{-5}	---	---	2.9×10^{-6}	---	1.1×10^{-6}	4.5×10^{-7}	2.7×10^{-7}	
39	3.4×10^{-7}	300	7.23×10^{-6}	3.62×10^{-6}	---	1.81×10^{-6}	1.27×10^{-6}	8.14×10^{-7}	4.5×10^{-7}	1.81×10^{-7}	
42A	1.8×10^{-7}	310	1.35×10^{-5}	---	---	2.0×10^{-6}	---	1.25×10^{-6}	---	5.2×10^{-7}	
48*	1.8×10^{-7}	300	1.12×10^{-5}	---	---	5.07×10^{-6}	---	4.06×10^{-5}	---	3.04×10^{-6}	Contaminated - particulate

Table 3. Continued

Run No.	Source		Scatter								Remarks
			Position, deg								
	Chamber Pressure, torr	Mirror Temperature, °K	1	2-1/3	3-2/3	5	6	8	12	16	
			BRDF/sr								
49*	7.0×10^{-7}	28	1.4×10^{-5}	---	---	4.9×10^{-6}	---	4.1×10^{-6}	3.3×10^{-6}	2.6×10^{-6}	Contaminated - particulate
63*	7.8×10^{-7}	27	2.3×10^{-5}	---	---	1.1×10^{-5}	---	9.8×10^{-6}	7.9×10^{-6}	6.8×10^{-6}	Contaminated - particulate
66*	3.8×10^{-7}	24	2.1×10^{-5}	---	---	1.4×10^{-5}	---	9.8×10^{-6}	7.3×10^{-6}	6.5×10^{-6}	Contaminated - particulate
72*	3.2×10^{-7}	22	4.2×10^{-5}	---	---	3.0×10^{-5}	---	2.6×10^{-5}	2.1×10^{-5}	1.7×10^{-5}	Contaminated - particulate
73*	2.9×10^{-7}	24	3.4×10^{-5}	---	---	2.3×10^{-5}	---	1.9×10^{-5}	1.7×10^{-5}	1.5×10^{-5}	Contaminated - particulate
75	3.5×10^{-7}	22	9.4×10^{-6}	4.2×10^{-6}	2.1×10^{-6}	1.8×10^{-6}	1.1×10^{-6}	5.9×10^{-7}	4.2×10^{-7}	3.4×10^{-7}	
79	3.3×10^{-7}	---	9.6×10^{-6}	4.4×10^{-6}	2.0×10^{-6}	1.6×10^{-6}	9.6×10^{-7}	5.6×10^{-7}	3.2×10^{-7}	1.6×10^{-7}	
82	1.9×10^{-7}	27	1.3×10^{-5}	3.9×10^{-6}	3.5×10^{-6}	2.0×10^{-6}	1.2×10^{-6}	1.0×10^{-6}	5.2×10^{-7}	2.6×10^{-7}	
88*	2.9×10^{-7}	24	5.82×10^{-5}	---	---	7.9×10^{-6}	---	3.33×10^{-6}	2.25×10^{-6}	1.83×10^{-6}	Warmed only to 108°K, some cryodeposit remains
90	2.4×10^{-7}	24	1.39×10^{-5}	3.8×10^{-6}	2.2×10^{-6}	1.47×10^{-6}	1.2×10^{-6}	8.16×10^{-7}	5.71×10^{-7}	2.45×10^{-7}	
94	1.8×10^{-7}	20	1.08×10^{-5}	3.6×10^{-6}	2.3×10^{-6}	1.54×10^{-6}	1.1×10^{-6}	7.23×10^{-7}	3.16×10^{-7}	1.81×10^{-7}	
100	2.5×10^{-7}	83	9.57×10^{-6}	3.3×10^{-6}	2.9×10^{-6}	1.66×10^{-6}	---	8.32×10^{-7}	4.99×10^{-7}	4.99×10^{-7}	
104	8.2×10^{-7}	300	7.5×10^{-6}	4.5×10^{-6}	2.5×10^{-7}	1.79×10^{-6}	1.2×10^{-6}	8.97×10^{-7}	5.71×10^{-7}	4.08×10^{-7}	
107*	7.8×10^{-7}	29	1.3×10^{-5}	7.8×10^{-6}	---	1.73×10^{-6}	1.73×10^{-6}	1.04×10^{-6}	8.67×10^{-7}	---	Contaminated
111	8.6×10^{-7}	365	8.85×10^{-6}	4.4×10^{-6}	2.4×10^{-6}	2.21×10^{-6}	1.3×10^{-6}	1.06×10^{-6}	7.08×10^{-7}	3.31×10^{-7}	Heated to 200°K, pattern of previous cryodeposit remains
113	4.4×10^{-7}	270	1.39×10^{-5}	5.6×10^{-6}	3.0×10^{-6}	1.73×10^{-6}	1.3×10^{-6}	1.04×10^{-6}	3.5×10^{-7}	4.3×10^{-7}	Pattern of previous cryodeposit disappeared (held at 100°K overnight)
116	3.3×10^{-7}	41	1.10×10^{-5}	4.2×10^{-6}	2.7×10^{-6}	1.70×10^{-6}	1.0×10^{-6}	1.02×10^{-6}	4.24×10^{-7}	2.55×10^{-7}	

Table 3. Continued

Run No.	Source		Scatter								Remarks
			Position, deg								
	Chamber Pressure, torr	Mirror Temperature, °K	1	2-1/3	3-2/3	5	6	8	12	16	
			BRDF/sr								
118	Not Recorded	30	1.09×10^{-5}	4.2×10^{-6}	2.3×10^{-6}	1.61×10^{-6}	1.0×10^{-6}	7.56×10^{-7}	5.7×10^{-7}	2.8×10^{-7}	
121*	1.3×10^{-6}	48	1.63×10^{-5}	2.71×10^{-6}	2.26×10^{-6}	4.52×10^{-7}	1.8×10^{-7}	---	1.8×10^{-7}	---	Telescope misaligned
123	1.4×10^{-6}	31	1.04×10^{-5}	3.8×10^{-6}	---	1.42×10^{-6}	1.32×10^{-6}	9.45×10^{-7}	---	2.8×10^{-7}	
125	1.4×10^{-6}	30	8.5×10^{-6}	3.8×10^{-6}	---	1.61×10^{-6}	1.3×10^{-6}	8.5×10^{-7}	---	4.72×10^{-7}	
127	1.5×10^{-6}	27	1.19×10^{-5}	4.5×10^{-6}	2.5×10^{-6}	1.59×10^{-6}	1.0×10^{-6}	8.9×10^{-7}	4.96×10^{-7}	4.96×10^{-7}	
129	Not Recorded	Cold, Not Recorded	1.2×10^{-5}	4.5×10^{-6}	3.0×10^{-6}	1.5×10^{-6}	1.3×10^{-6}	8.0×10^{-7}	6.0×10^{-7}	3.0×10^{-7}	
132	1.4×10^{-6}	23	1.1×10^{-5}	4.4×10^{-6}	2.8×10^{-6}	1.3×10^{-6}	1.1×10^{-6}	9.0×10^{-7}	4.0×10^{-7}	3.0×10^{-7}	
137	1.4×10^{-6}	26	1.06×10^{-5}	4.1×10^{-6}	---	1.45×10^{-6}	1.2×10^{-6}	8.73×10^{-7}	3.9×10^{-7}	3.87×10^{-7}	
145	1.1×10^{-6}	21	9.91×10^{-6}	4.3×10^{-6}	3.0×10^{-6}	1.68×10^{-6}	1.2×10^{-6}	7.93×10^{-7}	3.96×10^{-7}	2.97×10^{-7}	
149*	8.0×10^{-3}	300	6.75×10^{-5}	4.54×10^{-5}	3.38×10^{-5}	2.64×10^{-5}	2.32×10^{-5}	2.0×10^{-5}	1.27×10^{-5}	8.45×10^{-6}	Measurement of alternate test mirror
150	6.0×10^{-3}	300	8.92×10^{-6}	4.5×10^{-6}	3.7×10^{-6}	1.98×10^{-6}	1.1×10^{-6}	9.9×10^{-7}	3.96×10^{-7}	3.96×10^{-7}	
151	1.1×10^{-6}	28	1.17×10^{-5}	3.9×10^{-6}	3.4×10^{-6}	1.82×10^{-6}	1.0×10^{-6}	6.07×10^{-7}	4.34×10^{-7}	3.47×10^{-7}	
158	1.4×10^{-6}	27	1.09×10^{-5}	4.5×10^{-6}	3.0×10^{-6}	1.78×10^{-6}	1.3×10^{-6}	7.93×10^{-7}	4.95×10^{-7}	2.97×10^{-7}	
164	1.3×10^{-6}	27	9.9×10^{-6}	4.2×10^{-6}	4.0×10^{-6}	2.48×10^{-6}	1.0×10^{-6}	8.92×10^{-7}	4.95×10^{-7}	4.46×10^{-7}	
169	1.2×10^{-6}	27	1.0×10^{-5}	5.0×10^{-6}	3.1×10^{-6}	2.02×10^{-6}	1.2×10^{-6}	1.07×10^{-6}	6.72×10^{-7}	6.72×10^{-7}	
173	1.6×10^{-6}	50	1.08×10^{-5}	4.6×10^{-6}	3.2×10^{-6}	2.2×10^{-6}	1.5×10^{-6}	1.08×10^{-6}	8.0×10^{-7}	6.8×10^{-7}	
177*	1.4×10^{-6}	30	7.0×10^{-4}	3.5×10^{-4}	7.7×10^{-5}	5.9×10^{-5}	1.6×10^{-5}	1.48×10^{-5}	3.0×10^{-6}	3.7×10^{-6}	Incident beam not centered, incident beam 15 deg from normal, opposite telescope movement
178*	1.2×10^{-6}	30	8.6×10^{-6}	4.7×10^{-6}	3.5×10^{-6}	1.25×10^{-6}	2.0×10^{-6}	4.7×10^{-7}	63×10^{-7}	4.7×10^{-7}	Incident beam 15 deg from normal, opposite telescope movement

Table 3. Concluded

Run No.	Source		Scatter								Remarks
			Position, deg								
	Chamber Pressure, torr	Mirror Temperature, °K	1	2-1/3	3-2/3	5	6	8	12	16	
			BRDF/sr								
179A*	1.2×10^{-6}	24	1.25×10^{-5}	3.6×10^{-6}	2.9×10^{-6}	2.5×10^{-6}	1.66×10^{-6}	1.0×10^{-6}	5.0×10^{-7}	6.6×10^{-7}	Incident beam 6 1/2 deg from normal
179B*	1.2×10^{-6}	24	1.33×10^{-5}	4.1×10^{-6}	3.3×10^{-6}	---	1.66×10^{-6}	1.0×10^{-6}	6.6×10^{-7}	3.3×10^{-7}	Incident beam 6 1/2 deg from normal, opposite telescope movement
181*	atm	300	7.2×10^{-6}	8.1×10^{-6}	3.6×10^{-6}	1.81×10^{-6}	---	9.0×10^{-7}	---	---	Ambient conditions, chamber open, some contamination
182*	atm	300	6.1×10^{-6}	8.1×10^{-6}	3.7×10^{-6}	1.2×10^{-6}	---	1.2×10^{-6}	---	---	Ambient conditions, chamber open, some contamination
Mean value of BRDF		$\bar{x}$	1.06×10^{-5}	4.23×10^{-6}	2.84×10^{-6}	1.80×10^{-6}	1.17×10^{-6}	8.98×10^{-6}	4.89×10^{-7}	3.68×10^{-7}	
Number of samples		n	27	25	21	27	24	27	24	27	
Standard Deviation		σ	0.17×10^{-5}	0.48×10^{-6}	0.54×10^{-6}	0.35×10^{-6}	0.14×10^{-6}	1.70×10^{-7}	1.22×10^{-7}	1.38×10^{-7}	
95% confidence		$\frac{x_{.95}}{\bar{x}}$(%)	32	23	38	39	24	36	50	75	

*Runs were not used in calculating the mean and curve fit.

Table 4. N_2-Directed Flow Data

Run No.	Source		Mirror Temperature, °K	n	Thickness, μm	Deposition Rate, μm/min	Scatter					
							Position, deg					
	Temperature, °K	Pressure, torr	Dep/Meas				1	2 1/3	3 2/3	5	6	8
							BRDF/sr					
8	300	250	16	---	2.10	0.39	1.2×10^{-5}	4.4×10^{-6}	4.0×10^{-6}	---	1.2×10^{-6}	$6.4 \times$
8A	---	---	16	---	<2.10	---	2.5×10^{-5}	1.5×10^{-5}	1.3×10^{-5}	---	1.1×10^{-5}	$9.4 \times$
9	300	250	20	1.270	5.58	0.42	2.2×10^{-5}	5.2×10^{-6}	---	1.3×10^{-6}	---	---
10	300	250	19	1.269	15.18	0.44	1.4×10^{-5}	---	---	1.5×10^{-6}	7.7×10^{-7}	---
11	300	250	18	1.268	28.87	0.42	1.0×10^{-5}	---	---	1.5×10^{-6}	3.7×10^{-7}	---
13	300	650	20	---	5.69	Variable	1.0×10^{-5}	---	---	8.3×10^{-7}	8.3×10^{-7}	---
14	300	500	20	1.287	23.82		1.1×10^{-5}	5.2×10^{-6}	---	1.5×10^{-6}	1.5×10^{-6}	---
15	300	500	20	---	25.42	Variable	1.1×10^{-5}	6.0×10^{-6}	---	3.7×10^{-6}	---	---
120	300	250	29/22	1.254	1.43	Variable	1.0×10^{-5}	4.7×10^{-6}	2.6×10^{-6}	1.8×10^{-6}	1.4×10^{-6}	$9.4 \times$
122	300	250	30	1.150	7.00	0.37	2.0×10^{-5}	3.8×10^{-6}	1.0×10^{-6}	4.0×10^{-7}	3.0×10^{-7}	
145 (Bare)							9.9×10^{-6}	4.3×10^{-6}	3.0×10^{-6}	1.7×10^{-6}	1.2×10^{-6}	$7.9 \times$
146	300	250	22/21	1.221	6.12	0.44	1.0×10^{-5}	4.3×10^{-6}	2.7×10^{-6}	1.7×10^{-6}	1.2×10^{-6}	$8.9 \times$
147	---	---		---	≈3.0	---	5.7×10^{-5}	---	4.7×10^{-5}	4.5×10^{-5}	4.3×10^{-5}	$4.6 \times$
148	300	250	21/20	1.213	10.20	0.41	4.1×10^{-3}	4.05×10^{-3}	3.8×10^{-3}	3.7×10^{-3}	3.4×10^{-3}	$3.3 \times$
165	1,000	100	27	1.249	5.89	0.48	1.6×10^{-5}	5.0×10^{-6}	3.5×10^{-6}	2.0×10^{-6}	1.2×10^{-6}	$6.9 \times$
Bare							1.1×10^{-5}	4.2×10^{-6}	2.8×10^{-6}	1.8×10^{-6}	1.2×10^{-6}	$8.9 \times$

2

Flow Data

	8	12	16	Remarks
10^{-6}	6.4×10^{-7}	---	---	Prior deposit (not recorded) purged to 40°K, then deposit of run 8 laid
10^{-5}	9.4×10^{-6}	---	---	Deposit 8 partially purged to maximum scatter
	---	---	---	Purged to room temperature prior to deposit, invisible deposit
10^{-7}	---	---	---	Deposit added to run 9
10^{-7}	---	---	---	Deposit added to run 10
10^{-7}	---	---	---	Purged to 130°F prior to deposit, deposition conditions not constant
10^{-6}	---	4.5×10^{-7}	---	Purged to 130°F prior to deposit, some visible scatter
	---	---	---	Deposit added to run 14, deposition conditions not constant
10^{-6}	9.4×10^{-7}	4.2×10^{-7}	3.1×10^{-7}	Purged to 150°F prior to deposit, deposition conditions not constant, diffuse, white appearance, picture taken
10^{-7}				Diffuse, white appearance, scatter at large angles are invalid due to telescope misalignment
10^{-6}	7.9×10^{-7}	4.0×10^{-7}	3.0×10^{-7}	
10^{-6}	8.9×10^{-7}	5.4×10^{-7}	3.2×10^{-7}	Invisible deposit
10^{-5}	4.6×10^{-5}	4.8×10^{-5}	5.1×10^{-5}	Deposit of 146 partially purged, diffuse appearance
10^{-3}	3.3×10^{-3}	2.9×10^{-3}	2.6×10^{-3}	Deposit added to 147 rough, white appearance
10^{-6}	6.9×10^{-7}	6.9×10^{-7}	5.0×10^{-7}	Invisible deposit except for slight haze
10^{-6}	8.9×10^{-7}	4.9×10^{-7}	3.7×10^{-7}	

Table 5. O_2-Directed Flow D

Run No.	Source Temperature, °K	Source Pressure, torr	Mirror Temperature, °K Dep/Meas	Index of Refraction	Thickness, μm	Deposition Rate, μm/min	Scatter Position, deg 1	2-1/3	3-2/3	5	6
							BRDF/sr				
40	300	250	26/23	1.468	5.37	0.344	2.4×10^{-4}	2.3×10^{-4}	---	2.2×10^{-4}	2.2×10^{-4}
41	300	250	23	1.408	10.38	0.335	3.7×10^{-4}	3.6×10^{-4}	3.5×10^{-4}	3.5×10^{-4}	3.5×10^{-4}
42	300	250	23/22	1.310	5.31	0.328	6.8×10^{-5}	6.2×10^{-5}	---	5.8×10^{-5}	5.6×10^{-5}
42H (Bare)							1.35×10^{-5}	---	---	2.0×10^{-6}	---
43	300	115	26	---	0.54	0.165	1.45×10^{-5}	5.0×10^{-6}	---	2.7×10^{-6}	1.6×10^{-6}
44	300	115	23	---	0.21	0.155	1.35×10^{-5}	7.3×10^{-6}	---	4.2×10^{-6}	3.1×10^{-6}
45	300	115	22	1.295	2.89	0.147	2.6×10^{-5}	1.8×10^{-5}	1.6×10^{-5}	1.6×10^{-5}	1.6×10^{-5}
46	300	115	22/21	1.304	4.23	0.154	2.0×10^{-5}	1.55×10^{-5}	---	1.15×10^{-5}	1.1×10^{-5}
47	300	115	21	1.305	5.37	0.151	3.1×10^{-5}	2.5×10^{-5}	---	2.3×10^{-5}	2.2×10^{-5}
49 (Bare)							1.4×10^{-5}	7.2×10^{-6}	6.5×10^{-6}	4.9×10^{-6}	4.2×10^{-6}
50	300	250	24	1.356	1.28	0.339	$.5 \times 10^{-5}$	8.3×10^{-6}	6.9×10^{-6}	5.5×10^{-6}	4.9×10^{-6}
51	300	250	22	1.321	2.22	0.321	1.8×10^{-5}	9.5×10^{-6}	9.5×10^{-6}	8.0×10^{-6}	6.6×10^{-6}
52	300	250	22	1.323	3.22	0.317	1.6×10^{-5}	9.0×10^{-6}	9.0×10^{-6}	6.9×10^{-6}	6.2×10^{-6}
53	300	250	21/20	1.358	4.30	0.348	1.6×10^{-5}	8.6×10^{-6}	7.9×10^{-6}	5.7×10^{-6}	5.0×10^{-6}
54	300	250	20	1.323	5.24	0.313	1.9×10^{-5}	1.1×10^{-5}	1.1×10^{-5}	8.9×10^{-6}	7.4×10^{-6}
55	300	250	21	1.318	6.89	0.321	2.3×10^{-5}	1.4×10^{-5}	1.4×10^{-5}	1.2×10^{-5}	1.2×10^{-5}
56	300	250	21	1.304	8.60	0.320	2.1×10^{-5}	1.4×10^{-5}	1.3×10^{-5}	1.2×10^{-5}	1.1×10^{-5}
57	300	250	20	1.309	10.34	0.307	3.6×10^{-5}	2.4×10^{-5}	2.4×10^{-5}	2.2×10^{-5}	2.1×10^{-5}
58	300	250	20	1.305	12.02	0.320	2.1×10^{-5}	1.5×10^{-5}	1.5×10^{-5}	1.4×10^{-5}	1.4×10^{-5}
59	300	250	21/20	1.333	13.60	0.304	2.7×10^{-5}	2.4×10^{-5}	2.2×10^{-5}	2.1×10^{-5}	1.8×10^{-5}
60	300	250	20/22	1.326	15.32	0.329	2.7×10^{-5}	2.2×10^{-5}	1.9×10^{-5}	1.8×10^{-5}	1.6×10^{-5}
61	300	250	22/21	1.351	17.00	0.316	2.8×10^{-5}	2.2×10^{-5}	2.0×10^{-5}	1.9×10^{-5}	1.7×10^{-5}
62	300	250	21/20	1.351	18.64	0.308	5.4×10^{-5}	4.3×10^{-5}	4.6×10^{-5}	4.4×10^{-5}	3.8×10^{-5}
63 (Bare)							2.3×10^{-5}	1.4×10^{-5}	1.1×10^{-5}	1.1×10^{-5}	1.1×10^{-5}
75 (Bare)							9.4×10^{-6}	4.2×10^{-6}	2.1×10^{-6}	1.8×10^{-6}	1.1×10^{-6}
Bare Avg							1.1×10^{-5}	4.3×10^{-6}	2.8×10^{-6}	1.8×10^{-6}	1.2×10^{-6}

Directed Flow Data

Scatter					Remarks			
Position, deg								
5	6	8	12	16	Mirror Treatment Prior to Deposit	Appearance Prior to Deposit	Appearance of Deposit	Other
1989 [illegible]								
[illegible] $\times 10^{-4}$	2.9×10^{-4}	2.5×10^{-4}	2.7×10^{-4}	2.8×10^{-4}	Just cleaned	Clean	Diffuse	
[illegible] $\times 10^{-4}$	4.5×10^{-4}	4.0×10^{-4}	4.3×10^{-4}	4.1×10^{-4}			-	Added to 40
[illegible] $\times 10^{-5}$	5.6×10^{-5}	5.8×10^{-5}	5.6×10^{-5}	5.2×10^{-5}	Warmed to 520°K	Some visible scatter	Diffuse	
[illegible] $\times 10^{-6}$		1.25×10^{-6}		5.7×10^{-7}				
[illegible] $\times 10^{-6}$	1.6×10^{-6}	1.4×10^{-6}	-	9.0×10^{-7}	Warmed to 100[illegible]K	Clean	Diffuse	
[illegible] $\times 10^{-6}$	3.1×10^{-6}	3.1×10^{-6}	-	2.1×10^{-6}			-	Added to 43
[illegible] $\times 10^{-5}$	1.6×10^{-5}	1.5×10^{-5}	1.4×10^{-5}	1.1×10^{-5}				Added to 44
[illegible] $\times 10^{-5}$	1.1×10^{-5}	1.0×10^{-5}	1.0×10^{-5}	9.4×10^{-6}			-	Added to 45
[illegible] $\times 10^{-5}$	2.2×10^{-5}	2.1×10^{-5}	2.0×10^{-5}	2.0×10^{-5}				Added to 46
[illegible] $\times 10^{-6}$	4.2×10^{-6}	4.1×10^{-6}	4.3×10^{-6}	2.6×10^{-6}	Mirror did not clean up during purge			
[illegible] $\times 10^{-6}$	4.9×10^{-6}	4.9×10^{-6}	4.2×10^{-6}	3.5×10^{-6}	Warmed to 110°F	Some contamination	Barely visible	
[illegible] $\times 10^{-6}$	6.6×10^{-6}	6.6×10^{-6}	5.8×10^{-6}	5.5×10^{-6}			Diffuse	
[illegible] $\times 10^{-6}$	6.2×10^{-6}	5.3×10^{-6}	5.2×10^{-6}	1.5×10^{-6}			-	
[illegible] $\times 10^{-6}$	5.0×10^{-6}	1.9×10^{-6}	4.7×10^{-6}	4.3×10^{-6}			Diffuse	
[illegible] $\times 10^{-6}$	7.4×10^{-6}	7.1×10^{-6}	6.7×10^{-6}	5.9×10^{-6}				
[illegible] $\times 10^{-5}$	1.2×10^{-5}	1.2×10^{-5}	1.0×10^{-5}	9.5×10^{-6}				
[illegible] $\times 10^{-5}$	1.1×10^{-5}	1.1×10^{-5}	9.7×10^{-6}	7.6×10^{-6}			- - -	
[illegible] $\times 10^{-5}$	2.1×10^{-5}	2.1×10^{-5}	1.7×10^{-5}	1.5×10^{-5}				
[illegible] $\times 10^{-5}$	1.4×10^{-5}	1.2×10^{-5}	1.1×10^{-5}	8.9×10^{-6}				
[illegible] $\times 10^{-5}$	1.8×10^{-5}	1.8×10^{-5}	1.7×10^{-5}	1.5×10^{-5}				
[illegible] $\times 10^{-5}$	1.6×10^{-5}	1.7×10^{-5}	1.7×10^{-5}	1.4×10^{-5}				
[illegible] $\times 10^{-5}$	1.7×10^{-5}	1.7×10^{-5}	1.7×10^{-5}	1.4×10^{-5}				
[illegible] $\times 10^{-5}$	3.6×10^{-5}	3.9×10^{-5}	3.6×10^{-5}	3.1×10^{-5}				
[illegible] $\times 10^{-5}$	1.1×10^{-5}	9.8×10^{-6}	7.9×10^{-6}	6.8×10^{-6}				
[illegible] $\times 10^{-6}$	1.1×10^{-6}	5.9×10^{-7}	4.2×10^{-7}	3.1×10^{-7}				
[illegible] $\times 10^{-5}$	1.2×10^{-5}	8.3×10^{-7}	5.3×10^{-7}	3.6×10^{-7}				

Table 5. Concluded

	Run No.	Source Temperature, °K	Source Pressure, torr	Mirror Temperature, °K Dep/Mean	Index of Refraction	Thickness, μm	Deposition Rate, μm/min	Scatter Position, deg 1	2 1/3	3 2/3	5	6	
								BRDF/sr					
Contaminated	64	300	250	26/22	1.317	5.27	0.321	4.7×10^{-5}	4.2×10^{-5}	3.7×10^{-5}	3.9×10^{-5}	3.8×10^{-5}	3
	65	300	250	22/21	1.291	10.28	0.309	1.1×10^{-4}	1.0×10^{-4}	1.0×10^{-4}	9.5×10^{-5}	9.5×10^{-5}	9
	67	300	250	23/22	1.317	5.21	0.317	4.4×10^{-5}	3.8×10^{-5}	3.5×10^{-5}	3.5×10^{-5}	3.4×10^{-5}	3
	68	300	250	22/21	1.291	10.31	0.324	1.4×10^{-5}	1.4×10^{-4}	1.4×10^{-4}	1.4×10^{-4}	1.4×10^{-4}	1
	69	300	250	22/20	1.305	5.21	0.317	6.4×10^{-5}	6.3×10^{-5}	5.9×10^{-5}	5.9×10^{-5}	5.8×10^{-5}	5
	70	300	250	22/21	1.284	10.24	0.309	2.6×10^{-4}	2.8×10^{-4}	2.8×10^{-4}	2.7×10^{-4}	2.8×10^{-4}	2
	71	---	---	21	--	9.91	---	5.0×10^{-4}	4.8×10^{-4}	5.0×10^{-4}	5.0×10^{-4}	4.7×10^{-4}	4
	74	300	80	28/22, 21	1.328	5.24	0.067	6.5×10^{-5}	5.9×10^{-5}	5.5×10^{-5}	5.5×10^{-5}	5.2×10^{-5}	5
	75 (Bare)							9.4×10^{-6}	4.2×10^{-6}	2.1×10^{-6}	1.8×10^{-6}	1.1×10^{-6}	5
	76	300	250	22/21	1.307	5.21	0.257	5.9×10^{-5}	5.4×10^{-5}	5.4×10^{-5}	5.0×10^{-5}	4.9×10^{-5}	4
	77	300	250	22/21	1.300	10.24	0.250	1.4×10^{-4}	1.3×10^{-4}	1.4×10^{-4}	1.25×10^{-4}	1.2×10^{-4}	1
	78	300	250	22/21	1.313	15.32	0.244	1.0×10^{-4}	1.0×10^{-4}	1.0×10^{-4}	9.5×10^{-5}	1.0×10^{-4}	9
	79 (Bare)							9.6×10^{-6}	4.4×10^{-6}	2.0×10^{-6}	1.6×10^{-6}	9.6×10^{-7}	5
	80	300	250	32/28	1.321	5.27	0.257	1.4×10^{-4}	1.3×10^{-4}	1.25×10^{-4}	1.3×10^{-4}	1.2×10^{-4}	1
	81	---	---	23	--	~4.6	- -	9.0×10^{-5}	7.7×10^{-5}	7.4×10^{-5}	7.7×10^{-5}	7.2×10^{-5}	7
	82 (Bare)							1.3×10^{-5}	3.9×10^{-6}	3.5×10^{-6}	2.0×10^{-6}	1.2×10^{-6}	1
	123A	300	250	33	1.264	5.61	0.250						
	123 (Bare)							1.0×10^{-5}	3.8×10^{-6}		1.4×10^{-6}	1.3×10^{-6}	9
	124	300	250	33/23	1.270	5.57	0.270	4.6×10^{-4}	4.3×10^{-4}		4.1×10^{-4}	4.1×10^{-4}	3
	125 (Bare)							8.5×10^{-6}	3.8×10^{-6}		1.6×10^{-6}	1.3×10^{-6}	8
	166	1,000	100	26	1.310	5.30	0.343	3.3×10^{-5}	2.1×10^{-5}	2.0×10^{-5}	2.0×10^{-5}	1.8×10^{-5}	1
	167	1,000	100	26/25	1.294	10.40	0.341	8.1×10^{-5}	6.1×10^{-5}	6.4×10^{-5}	5.9×10^{-5}	5.9×10^{-5}	5
	168	1,000	100	26/25	1.305	15.74	0.330	4.4×10^{-5}	3.4×10^{-5}	3.5×10^{-5}	3.2×10^{-5}	3.3×10^{-5}	3
								1.0×10^{-5}	5.0×10^{-6}	7.1×10^{-6}	2.0×10^{-6}	1.2×10^{-6}	1
	Bare Avg.							1.1×10^{-5}	4.3×10^{-6}	2.8×10^{-6}	1.8×10^{-6}	1.2×10^{-6}	8.5

5. Concluded

Scatter position, deg					Remarks			
	6	8	12	16				
BRDF	Sr				Mirror Treatment Prior to Deposit	Appearance Prior to Deposit	Appearance of Deposit	Other
10^{-5}	3.8×10^{-5}	3.6×10^{-5}	3.3×10^{-5}	4.0×10^{-5}	Heated to 140°F	Contaminated	---	
10^{-5}	9.5×10^{-5}	9.5×10^{-5}	7.9×10^{-5}	7.9×10^{-5}		---	---	Added to 64
10^{-5}	3.4×10^{-5}	3.3×10^{-5}	3.4×10^{-5}	3.1×10^{-5}	Held at 80°F overnight	Contaminated	Diffuse, white	
10^{-4}	1.4×10^{-4}	1.4×10^{-4}	1.3×10^{-4}	1.3×10^{-4}		---	Diffuse	Added to 67
10^{-5}	5.6×10^{-5}	5.3×10^{-5}	5.3×10^{-5}	4.8×10^{-5}	Heated to 48°K	Contaminated	Diffuse, brown	
10^{-4}	2.8×10^{-4}	2.6×10^{-4}	2.8×10^{-4}	2.6×10^{-4}	---	---	Diffuse, brown	Added to 69
10^{-4}	4.7×10^{-4}	4.8×10^{-4}	4.5×10^{-4}	4.2×10^{-4}	Small part of 70 purged	---	---	
10^{-5}	5.2×10^{-5}	5.1×10^{-5}	4.6×10^{-5}	4.2×10^{-5}	Heated to 130°F	Contaminated		
10^{-6}	1.1×10^{-6}	5.9×10^{-7}	4.2×10^{-7}	3.4×10^{-7}				
10^{-5}	4.9×10^{-5}	4.6×10^{-5}	3.7×10^{-5}	3.0×10^{-5}	Clean Mirror	Clean	Diffuse, white	
10^{-4}	1.2×10^{-4}	1.2×10^{-4}	1.2×10^{-4}	1.1×10^{-4}	---	---	Diffuse, brown	Added to 76
10^{-5}	1.0×10^{-4}	9.5×10^{-5}	1.0×10^{-4}	1.0×10^{-4}	---	---	Diffuse, brown	Added to 77
10^{-6}	8.6×10^{-7}	5.6×10^{-7}	3.2×10^{-7}	1.6×10^{-7}				
10^{-4}	1.2×10^{-4}	1.2×10^{-4}	1.1×10^{-4}	1.1×10^{-4}	Heated to 60°F	Clean	---	
10^{-5}	7.2×10^{-5}	7.2×10^{-5}	7.2×10^{-5}	6.8×10^{-5}	Small part of 80 purged	---	Diffuse, brown	
10^{-6}	1.2×10^{-6}	1.0×10^{-6}	5.2×10^{-7}	2.6×10^{-7}				
					Heated to 125°F	Clean	Diffuse, brown	Telescope misaligned
10^{-6}	1.3×10^{-6}	9.5×10^{-7}						
10^{-4}	4.1×10^{-4}	3.9×10^{-4}	3.6×10^{-4}	3.5×10^{-4}	Heated to 130°F	Clean	Diffuse, brown	
10^{-6}	1.3×10^{-6}	8.5×10^{-7}		4.7×10^{-7}				
10^{-5}	1.8×10^{-5}	1.7×10^{-5}	1.7×10^{-5}	1.7×10^{-5}	Heated to 140°F	Clean	Diffuse, white	
10^{-5}	5.9×10^{-5}	5.7×10^{-5}	5.7×10^{-5}	5.8×10^{-5}	---	---	Diffuse, white	Added to 167
10^{-5}	3.1×10^{-5}	3.1×10^{-5}	3.2×10^{-5}	3.3×10^{-5}	---	---	Diffuse, white	Added to 168
10^{-6}	1.2×10^{-6}	1.1×10^{-6}	6.7×10^{-7}	6.7×10^{-7}				
10^{-6}	1.2×10^{-6}	8.9×10^{-7}	5.3×10^{-7}	3.6×10^{-7}				

Table 6. CO_2-Directed

Run No.	Source Temperature, °K	Source Pressure, torr	Mirror Temperature, °K Dep/Meas	Index of Refraction	Thickness, μm	Deposition Rate, μm/min	Scatter Position, deg 1	2-1/3	3-2/3	5	6	8
							BRDF/sr					
83	300	250	27	1.368	4.99	0.34	1.1×10^{-5}	6.9×10^{-6}	4.3×10^{-6}	2.6×10^{-6}	2.2×10^{-6}	2.2×10
84			26/25	1.348	9.76	0.32	7.6×10^{-5}	7.2×10^{-5}	6.1×10^{-5}	7.2×10^{-5}	4.6×10^{-5}	3.8×10
85			25	1.358	1.56	0.30	4.7×10^{-5}	3.4×10^{-5}	2.9×10^{-5}	2.9×10^{-5}	2.5×10^{-5}	3.0×10
86			26/25	1.334	19.36	0.29	7.8×10^{-5}	4.0×10^{-5}	3.3×10^{-5}	3.0×10^{-5}	2.8×10^{-5}	3.6×10
87			---	---	≈16.0	---	1.2×10^{-1}	4.3×10^{-2}	4.2×10^{-2}	4.2×10^{-2}	4.2×10^{-2}	3.9×10
88 (Bare)			108		0		5.8×10^{-5}	2.08×10^{-5}	1.0×10^{-5}	7.9×10^{-6}	4.2×10^{-6}	3.3×10
89			21	---	≈8.0	≈0.34	3.9×10^{-2}	---	---	5.2×10^{-2}	4.8×10^{-2}	4.6×10
91			21	1.302	1.94	0.28	1.0×10^{-5}	4.5×10^{-6}	1.8×10^{-6}	1.8×10^{-6}	9.0×10^{-7}	9.0×10
92			21/20	1.287	3.87	0.27	9.1×10^{-6}	3.3×10^{-6}	2.5×10^{-6}	2.1×10^{-6}	1.25×10^{-6}	1.25×1
93			21/20	1.283	5.43	0.26	1.0×10^{-5}	4.3×10^{-6}	2.6×10^{-6}	1.7×10^{-6}	1.3×10^{-6}	1.3×10
90			21/20	1.348	4.96	0.35	1.1×10^{-5}	3.7×10^{-6}	2.3×10^{-6}	1.9×10^{-6}	1.4×10^{-6}	9.2×10
96			21	1.343	6.59	0.34	1.0×10^{-5}	4.3×10^{-6}	2.6×10^{-6}	1.7×10^{-6}	1.3×10^{-6}	1.3×10
97			21/20	1.344	8.19	0.34	1.7×10^{-5}	1.2×10^{-5}	7.8×10^{-6}	8.2×10^{-6}	6.5×10^{-6}	6.5×10
98			21/20	1.332	9.76	0.33	2.0×10^{-4}	1.6×10^{-4}	1.4×10^{-4}	1.3×10^{-4}	1.2×10^{-4}	1.1×10
99			21/30	1.330	14.62	0.33	2.2×10^{-4}	2.0×10^{-4}	1.9×10^{-4}	1.7×10^{-4}	1.7×10^{-4}	1.6×10
101			80, 71/83	1.370	4.96	0.28	8.3×10^{-6}	5.4×10^{-6}	2.3×10^{-6}	1.8×10^{-6}	1.3×10^{-6}	7.5×10
102			73/76, 76	1.348	9.76	0.28	1.2×10^{-5}	---	2.8×10^{-6}	2.2×10^{-6}	1.1×10^{-6}	6.9×10
103			---	---	9.76	---	7.6	1.15	0.381	0.24	0.15	0.12
Bare Ag							1.1×10^{-5}	4.3×10^{-6}	2.8×10^{-6}	1.8×10^{-6}	1.2×10^{-6}	8.5×10

e C. CO_2-Direc ed Flow Data

...ter, deg					Remarks			
6	8	12	16	Mirror Treatment Prior to Deposit	Appearance Prior to Deposit	Appearance of Deposit	Other
st							
2.2×10^{-6}	2.2×10^{-6}	2.6×10^{-6}	4.1×10^{-6}	Heated to 400°F	Clean	Diffuse, white	
4.6×10^{-5}	3.8×10^{-5}	2.4×10^{-5}	2.5×10^{-5}	"	"	Diffuse	Added to 83
2.5×10^{-5}	3.0×10^{-5}	3.2×10^{-5}	4.3×10^{-5}	"	"	Diffuse	Added to 84
2.8×10^{-5}	3.6×10^{-5}	3.7×10^{-5}	4.5×10^{-5}	"	"	Diffuse, white	Added to 85
3.2×10^{-2}	3.9×10^{-2}	3.5×10^{-2}	3.3×10^{-2}	"	"	Rough, brown	Removed part of 86
4.7×10^{-6}	3.3×10^{-6}	2.3×10^{-6}	1.8×10^{-6}				Heated 86 to 108°K
4.8×10^{-2}	4.8×10^{-2}	4.2×10^{-2}	3.5×10^{-2}	Heated to 108°K	Some visible scatter	Dull, grey	White film remained after purging 89
9.0×10^{-7}	9.0×10^{-7}	1.0×10^{-7}	-	Heated to 150°F	Clean	Slightly haze	
1.25×10^{-6}	1.25×10^{-6}	1.25×10^{-6}	8.7×10^{-7}	"	"	Milky center	Added to 91
1.3×10^{-6}	1.3×10^{-6}	8.7×10^{-7}	6.9×10^{-7}	"	"	"	Added to 92
1.4×10^{-6}	9.2×10^{-7}	4.6×10^{-7}	5.6×10^{-7}	Heated to 175°F for 24 hr	Clean	Diffuse, white	
1.3×10^{-6}	1.3×10^{-6}	1.3×10^{-6}	1.3×10^{-6}	"	"	Diffuse, white	Added to 95
6.5×10^{-6}	6.5×10^{-6}	4.3×10^{-5}	3.9×10^{-6}			Diffuse, white	Added to 96
1.2×10^{-4}	1.1×10^{-4}	6.1×10^{-5}	4.9×10^{-5}			Diffuse, white	Added to 97
1.7×10^{-4}	1.6×10^{-4}	1.3×10^{-4}	1.0×10^{-4}	"	"	Diffuse, white	Added to 98
1.3×10^{-6}	7.0×10^{-7}	5.3×10^{-7}	3.5×10^{-7}	Heated to 130°F	Clean	Slight haze	
1.1×10^{-6}	6.9×10^{-7}	4.3×10^{-7}	3.5×10^{-7}	"	"	White, hazy	Added to 101
0.15	0.12	0.026	0.012	Deposit of 102 Cooled to 60°K	"	Shattered	
1.2×10^{-6}	8.5×10^{-7}	5.3×10^{-7}	3.8×10^{-7}				

Table 7. NH_3-Directed

Run No.	Source		Mirror Temperature, °K Dep/Meas	Index of Refraction	Thickness, μm	Deposition Rate, μm/min	Scatter Position, deg				
	Temperature, °K	Pressure, torr					1	2-1/3	3-2/3	5	6
							BPH, sr				
105	300	200	27	1.382	4.85	0.25	0.7×10^{-4}	---	---	$2.3 \times 10^{-}$	$1.6 \times 10^{-}$
106	300	200	27/24	1.305	1.93	0.24	3.1	---	---	0.80	0.46
108	300	200	23	1.282	2.32	0.23	1.2×10^{-5}	5.2×10^{-6}	---	1.7×10^{-6}	---
109	300	200	22/21	---	3.75	≈0.23	79.0	---	---	2.54	1.44
110	300	200	23	---	4.88	≈0.23	48.5	---	---	2.85	1.74
112	300	200	77/72	1.265	5.59	0.18	1.4×10^{-5}	---	---	2.4×10^{-6}	2.4×10^{-6}
114	300	200	51/52	1.547	3.95	0.21	1.4×10^{-5}	5.2×10^{-6}	5.0×10^{-6}	3.6×10^{-6}	2.6×10^{-6}
115	300	200	51/52	1.569	7.81	0.19	1.7×10^{-5}	8.4×10^{-6}	6.8×10^{-6}	5.7×10^{-6}	4.4×10^{-6}
117	300	200	37/40,36	1.168	5.01	0.30	29.5	---	---	2.0	1.03
119	300	50	26	1.430	2.16	0.08	2.0	0.63	---	0.14	0.105
152	1,000	250	23	1.391	4.73	0.80	9.9×10^{-6}	4.4×10^{-6}	3.7×10^{-6}	1.7×10^{-6}	1.4×10^{-6}
153	1,000	399	24/23	1.398	9.47	0.32	9.9×10^{-6}	3.5×10^{-6}	2.9×10^{-6}	2.5×10^{-6}	9.8×10^{-7}
154	---	---	50	---	≈4.7	---	9.64	0.38	0.24	0.14	0.12
155	1,000	100	74/67	1.412	4.67	0.31	6.0×10^{-5}	2.7×10^{-5}	2.2×10^{-5}	1.6×10^{-5}	1.4×10^{-5}
156	1,000	100	67/64	1.389	9.57	0.32	1.2×10^{-4}	5.8×10^{-5}	4.8×10^{-5}	3.7×10^{-5}	3.5×10^{-5}
157	---	---	23	---	unknown		5.6×10^{-1}	2.4×10^{-1}	8.3×10^{-2}	2.3×10^{-2}	6.9×10^{-3}
160	300	≈100	23	1.334	2.12	variable	19.7	---	---	2.55	1.34
Burn Avg							1.1×10^{-5}	4.3×10^{-6}	2.8×10^{-6}	1.8×10^{-6}	1.7×10^{-6}

Table 7. NH_3-Directed Flow Data

Scatter Position, deg					Remarks			
5	6	8	12	16	Mirror Treatment Prior to Deposit	Appearance Prior to Deposit	Appearance of Deposit	Other
2.3 x 10^{-4}	1.6 x 10^{-4}	5.3 x 10^{-5}	6.0 x 10^{-5}	6.3 x 10^{-5}	Cleaned, first cooldown	Clean	Crystalline	
0.80	0.46	0.28	0.15	0.90	Heated to 150°F	Clean	Crystalline	Sudden change during deposition
1.7 x 10^{-6}		8.7 x 10^{-7}	8.7 x 10^{-7}	6.9 x 10^{-7}	Heated to 140°F	Clean	Small hairline crystals, aligned	Picture taken
2.54	1.44	0.71	0.27	0.11	"		Crystalline	Picture taken, added to 108
2.8	1.74	0.96	0.29	0.18	"		Crystalline	Picture taken, added to 109
2.4 x 10^{-6}	2.4 x 10^{-6}	2.1 x 10^{-6}	1.6 x 10^{-6}	1.0 x 10^{-6}	Heated to 200°F	Some particles remain after purge	Invisible	Slight haze after CO_2 purge
3.6 x 10^{-6}	2.6 x 10^{-6}	2.1 x 10^{-6}	1.9 x 10^{-6}	1.9 x 10^{-6}	Heated to 100°F for 24 hr	Clean	Invisible	
5.7 x 10^{-6}	4.4 x 10^{-6}	4.4 x 10^{-6}	3.8 x 10^{-6}	3.8 x 10^{-6}	"	"	Barely visible	Added to 114
2.0	1.03	0.37	0.17	0.090	Heated to 140°F	Clean	Shattered	Crystal pattern remained to 100°F
0.14	0.105	0.038	0.013	0.0052	Heated to 180°F	Clean	Crystalline	
1.7 x 10^{-6}	1.4 x 10^{-6}	9.9 x 10^{-7}	9.9 x 10^{-7}	3.9 x 10^{-7}	Cleaned, first cooldown	Clean	Invisible	
2.5 x 10^{-6}	9.9 x 10^{-7}	6.9 x 10^{-7}	5.0 x 10^{-7}	4.0 x 10^{-7}	"	"	Slightly diffuse, brown	Added to 152
0.14	0.12	0.050	0.029	0.015	Heated 153 to 60°K		Diffuse, white	Sudden change
1.6 x 10^{-5}	1.4 x 10^{-5}	1.3 x 10^{-5}	1.1 x 10^{-5}	9.8 x 10^{-6}	Heated to 70°F	Clean	Slightly diffuse	
3.7 x 10^{-5}	3.5 x 10^{-5}	3.2 x 10^{-5}	3.0 x 10^{-5}	2.8 x 10^{-5}		"	"	Added to 155
9.3 x 10^{-2}	6.9 x 10^{-3}	2.5 x 10^{-3}	1.0 x 10^{-3}	4.6 x 10^{-4}	Heated 156 to 80°K, then cooled to 48°K		Crystalline, climax in center	Shattered at 46°, most fell off
2.55	1.34	0.70	0.24	0.18	Heated to 150°F	Clean	Crystalline	Rate not constant, thickness unknown
1.8 x 10^{-6}	1.2 x 10^{-6}	8.5 x 10^{-7}	5.3 x 10^{-7}	3.6 x 10^{-7}				

Table 8. Directed Flow Data—CO, Air, an

Run No.	Gas	Source Temperature, °K	Source Pressure, torr	Mirror Temperature, °K Dep/Meas	Index of Refraction	Thickness, μm	Deposition Rate, μm/min	Scatter Position, deg 1	2-1/3	3-2/3	5	6	8
								BRDF/sr					
126	CO	300	250	27/24, 23	---	5.79	Variable	9.1×10^{-6}	3.9×10^{-6}	2.7×10^{-6}	2.0×10^{-6}	1.2×10^{-6}	8.1×10^{-7}
128	CO	300	250	31/30	1.237	5.79	0.37	1.3×10^{-5}	4.7×10^{-6}	3.6×10^{-6}	2.1×10^{-6}	1.8×10^{-6}	1.5×10^{-6}
130	CO	300	50	21/24, 21	1.277	5.50	0.08	1.0×10^{-5}	4.5×10^{-6}	3.0×10^{-6}	1.5×10^{-6}	1.2×10^{-6}	1.2×10^{-6}
131	Air	300	250	28/26, 25	1.208	6.34	0.34	9.0×10^{-6}	4.0×10^{-6}	2.7×10^{-6}	1.7×10^{-6}	1.2×10^{-6}	1.0×10^{-6}
133	Air	300	250	38/38	---	---	---	1.2×10^{-5}			1.5×10^{-6}	1.1×10^{-6}	9.0×10^{-7}
134	Air	300	250	33/39	1.215	1.83	0.038	1.3×10^{-5}	5.2×10^{-6}	---	1.8×10^{-6}	1.4×10^{-6}	1.0×10^{-6}
135	Air	300	50	26/21, 20	1.253	5.74	0.077	1.1×10^{-5}	---	---	1.7×10^{-6}	1.0×10^{-6}	7.0×10^{-6}
136	Air	300	---	21	---	---	---	6.2×10^{-5}	5.5×10^{-5}	---	5.2×10^{-5}	---	5.5×10^{-5}
160	H_2O	300	20	27	1.351	3.17	0.10	1.45	0.28	---	4.9×10^{-2}	3.5×10^{-2}	2.0×10^{-2}
160	H_2O	300	20	74/69	1.360	4.81	0.10	6.0×10^{-6}	3.2×10^{-6}	2.5×10^{-6}	2.0×10^{-6}	9.9×10^{-7}	7.9×10^{-7}
161	H_2O	1,000	0	27/24	1.373	4.72	0.065	6.4×10^{-6}	3.0×10^{-6}	2.3×10^{-6}	2.2×10^{-6}	9.9×10^{-7}	$6.[illegible] \times 10^{-7}$
162	H_2O	---	---	175°F	---	---	---	7.61	1.45	0.37	0.[illegible]58	0.101	0.945
163	H_2O	300	20	37/40, 37	1.378	4.77	0.08	4.0×10^{-6}	2.3×10^{-6}	1.8×10^{-6}	5.0×10^{-7}	4.0×10^{-7}	3.0×10^{-7}

Bare Avg

rected Flow Data–CO, Air, and H_2O

Scatter Position, deg					Remarks			
5	6	8	12	16	Mirror Treatment Prior to Deposit	Appearance Prior to Deposit	Appearance of Deposit	Other
BRDF, sr								
2.0×10^{-6}	1.2×10^{-6}	8.1×10^{-7}	5.0×10^{-7}	4.0×10^{-7}	Heated to 150°F	Clean	Invisible	
2.1×10^{-6}	1.8×10^{-6}	1.5×10^{-6}	8.3×10^{-7}	6.7×10^{-7}	Heated to 150°F	Clean	Diffuse, brown	
1.5×10^{-6}	1.2×10^{-6}	1.2×10^{-6}	5.0×10^{-7}	2.0×10^{-7}	Heated to 130°F	Clean	Invisible	
1.7×10^{-6}	1.2×10^{-6}	1.0×10^{-6}	4.0×10^{-7}	4.0×10^{-7}	Heated to 130°F	Clean	Bluish, nearly invisible	
1.5×10^{-6}	1.1×10^{-6}	9.0×10^{-7}	4.0×10^{-7}	3.0×10^{-7}	Heated to 100°F for 24 hr	Clean	Invisible	N_2 + O_2 not pumped [CO_2, Ar, H_2O]
1.8×10^{-6}	1.4×10^{-6}	1.0×10^{-6}	5.2×10^{-7}	5.2×10^{-7}	Heated to ~80°F	Clean	Clear with interference rings	N_2 not pumped
1.7×10^{-6}	1.0×10^{-6}	7.0×10^{-6}	4.0×10^{-7}	4.0×10^{-7}	Heated to 130°F	Clean	Invisible	
2.2×10^{-5}	---	3.5×10^{-5}	6.8×10^{-5}	7.1×10^{-5}	135 not completely purged	---	Diffuse, white	
4.9×10^{-2}	3.5×10^{-2}	2.0×10^{-2}	5.1×10^{-3}	2.9×10^{-3}	Heated to 150°F	Clean	Crystalline in spots	Shattered during deposition
2.0×10^{-6}	9.9×10^{-7}	7.9×10^{-7}	4.0×10^{-7}	4.0×10^{-7}	Heated to 130°F	Clean	Invisible	Cooled to 32°K, warmed to purge with no changes
2.2×10^{-6}	1.9×10^{-6}	2.0×10^{-6}	6.0×10^{-7}	1.0×10^{-6}	Heated to 130°F	Clean	Invisible	Shattered on warmup at 120°K
0.156	0.101	0.048	0.016	0.0069	161 after shattering	---	Crystalline	Crystal pattern remained to 500°F
5.0×10^{-7}	4.0×10^{-7}	3.0×10^{-7}	1.0×10^{-7}	2.0×10^{-7}	Heated to 140°F	Clean	Invisible	Warmed to purge with no changes

Table 9. Directed Flow Data—M

Run No	Gas Mixture	Source Temperature, °K	Source Pressure, torr	Mirror Temperature, °K Dep Meas	Gases Deposited	n	Thickness, μm	Deposition Rate, μm/min	λ	2 1 3	3 2/3	Scatter Position, deg 5	Scatter Position, deg 6	BRDF sr
138	1	300	250	28/23	N_2, NH_3	1.234	5.08	0.38	1.1×10^{5}	4.5×10^{6}		1.9×10^{6}		
139	1	300	250	49 44	NH_3	1.296	2.59	0.086	1.2×10^{5}	6.0×10^{6}	3.8×10^{6}	3.3×10^{6}	2.2×10^{6}	
140	2	300	250	26/22, 21	N_2, NH_3	1.231	5.95	0.35	5×10^{5}	1.7×10^{6}	3.6×10^{6}	1.7×10^{6}	1.2×10^{6}	
141	2			39	NH_3				7.1			1.65	1.20	
142	2	300	250	35 31	NH_3	1.261	1.59	0.13	4.0			0.61	0.44	
143	3	300	250	27/25, 22	N_2, NH_3	1.240	5.86	0.31	1.0×10^{5}	5.2×10^{6}	2.8×10^{6}	1.7×10^{6}	1.2×10^{6}	
144	3	300	250	23/21	N_2, NH_3		11.37	0.29	9.9×10^{5}	3.7×10^{6}	2.8×10^{6}	1.8×10^{6}	1.2×10^{6}	
170	3	300	3.2	27 24	All	1.276	5.31	0.10	1.28×10^{5}	4.0×10^{6}	3.1×10^{6}	2.4×10^{6}	1.1×10^{6}	
171	4	---	---	41	CO_2, H_2O		---		1.90	1.80	1.51	1.13	0.94	
172	4	300	3.5	30/32, 40	CO_2, H_2O	1.69	3.04	0.04	8.4×10^{6}	3.4×10^{6}	2.7×10^{6}	1.9×10^{6}	9.5×10^{7}	
174	4	1,000	6.5	27.24	All	1.300	1.23	0.07	9.5×10^{6}	4.0×10^{6}	3.0×10^{6}	1.6×10^{6}	1.1×10^{6}	
175	4	-		39	CO_2, H_2O	-	---	---	2.9			0.86	0.50	
176	4		---	34	CO, CO_2, H_2O	---	---		0.75	-		0.20	0.13	

Mixtures:
1. 60% N_2, 40% NH_3
2. 55% N_2, 45% NH_3
3. 33% N_2, 67% NH_3
4. 3.8% CO, 11% CO_2, 39% N_2, 47% H_2O

2

9. Directed Flow Data—Mixtures

Scatter Position, deg					Remarks			
2 3	5	6	8	12	16	Mirror Treatment Prior to Deposit	Appearance Prior to Deposit	Appearance of Deposit	Other
	10K0 sr							
	1.9×10^{-6}		1.0×10^{-6}	4.5×10^{-7}	3.3×10^{-7}	Held at 100°F overnight	Clean	Clear with interference rings	
8×10^{-6}	4.3×10^{-6}	2.2×10^{-6}	2.1×10^{-6}	1.7×10^{-6}	1.7×10^{-6}	Heated to 130°F	Clean	Invisible	Blue film at 130°K after purge, N_2 not pumped
4×10^{-6}	1.7×10^{-6}	1.2×10^{-6}	9.4×10^{-7}	5.2×10^{-7}	5.2×10^{-7}	Heated to 130°F	Clean	Clear with interference rings	Shattered during slow warmup as N_2 evaporated
	1.65	1.20	0.72	0.36	0.18	140 after shattering		Crystalline	
	0.61	0.44	0.25	0.115	0.069	Heated to 130°F	Clean	Crystalline	Shattered during deposition, N_2 not pumped
8×10^{-6}	1.7×10^{-6}	1.2×10^{-6}	9.1×10^{-7}	4.0×10^{-7}	4.0×10^{-7}	Heated to 80°F	Clean	Barely visible	
8×10^{-6}	1.8×10^{-6}	1.2×10^{-6}	8.9×10^{-7}	5.0×10^{-7}	4.0×10^{-7}			Barely visible	Added to 143, shattered during warmup as N_2 purged
4×10^{-6}	2.1×10^{-6}	1.1×10^{-6}	8.0×10^{-7}		5.4×10^{-7}	Held at 100°F overnight	Clean	Invisible	Crystallized on warmup to 41°K
31	1.11	0.94	0.86	0.28	0.17	170 after crystallization		Crystalline	
7×10^{-6}	1.9×10^{-6}	9.5×10^{-7}	5.4×10^{-7}	5.4×10^{-7}	5.4×10^{-7}	Heated to 150°F	Clean	Invisible	Cooled to 39°K with no change
						Color changes as CO_2 vaporized, diffuse, white as H_2O vaporized			
8×10^{-6}	1.6×10^{-6}	1.4×10^{-6}	9.4×10^{-7}	6.8×10^{-7}	6.8×10^{-7}	Held at 100°F overnight	Clean	Invisible	Shattered at 43°K on warmup, particles and pieces of film fell off
	0.83	0.59	0.27	0.10	0.042	174 after shattering		Crystalline	Crystal imprint remained to 45°K
	0.20	0.13	0.0	0.023	0.0145				175 at 5-deg in clined angle, laser not well centered on mirror

Table 10. Random Incidence N_2 and O_2

Run No.	Gas	Source Temperature, °K	Source Test Section Pressure, torr	Mirror Temperature, °K Dep/Beam	n	Thickness, μm	Deposition Rate μm/min	Scatter Position, deg 1	2 1/3	3 2/3	5	6	8
								BRDF sr					
16	[illegible]	~300	4.0×10^{-4}	20	1.217	9.89	1.433	1.5×10^{-4}			1.4×10^{-4}	1.4×10^{-4}	1.25×10
18	N_2		9.0×10^{-6}	19				1.4×10^{-5}	5.0×10^{-6}		- -	2.1×10^{-6}	
19	N_2		2.0×10^{-6} 4.0×10^{-6}	20			Variable	1.1×10^{-5}	5.7×10^{-6}	5.2×10^{-6}	----	3.0×10^{-6}	
20	N_2		4.0×10^{-6}	20				1.8×10^{-5}	1.0×10^{-5}	1.0×10^{-5}	8.9×10^{-6}	7.4×10^{-6}	
22	N_2		1.1×10^{-4}	22	1.224	12.32	0.22	1.4×10^{-5}	8.8×10^{-6}		5.8×10^{-6}	4.4×10^{-6}	4.0×10^{-6}
23	N_2		3.0×10^{-4}	26	1.216	12.32	0.81	3.6×10^{-5}	8.0×10^{-5}	--	1.4×10^{-5}	1.4×10^{-5}	1.2×10^{-5}
24	N_2		6.0×10^{-4}	26/23	1.223	12.01	1.97	2.6×10^{-5}	9.8×10^{-5}		6.1×10^{-6}	4.9×10^{-6}	4.1×10^{-6}
25	N_2		6.0×10^{-4}	23/21	-	~12.1	~1.97	2.6×10^{-3}	2.4×10^{-3}		2.0×10^{-3}	2.0×10^{-3}	2.4×10^{-3}
26	N_2		3.0×10^{-4}	25/22	1.221	12.36	0.62	8.6×10^{-6}	-		5.5×10^{-6}	3.9×10^{-6}	3.5×10^{-6}
27	N_2		3.0×10^{-4}	22/21	1.216	16.27	0.81	2.0×10^{-5}	1.0×10^{-5}	-	8.4×10^{-6}	6.4×10^{-6}	6.8×10^{-6}
28			3.0×10^{-4}	21	1.217	24.48	0.76	4.7×10^{-5}	3.3×10^{-5}	--	3.0×10^{-5}	2.8×10^{-5}	2.9×10^{-5}
29	N_2		3.0×10^{-4}	26/23	1.216	12.36	0.67	2.2×10^{-5}	2.0×10^{-5}	-	1.6×10^{-5}	1.4×10^{-5}	1.4×10^{-5}
30	N_2		3.0×10^{-4}	23/22	-	~12.1	~0.67	4.8×10^{-4}	4.0×10^{-4}	--	4.2×10^{-4}	4.8×10^{-4}	4.2×10^{-4}
32	N_2		3.0×10^{-4}	23/22	1.217	12.38	0.69	3.1×10^{-5}	1.4×10^{-5}		6.9×10^{-6}	5.4×10^{-6}	5.4×10^{-6}
Bare								1.1×10^{-5}	4.3×10^{-6}	2.8×10^{-6}	1.8×10^{-6}	1.2×10^{-6}	8.8×10^{-7}
33	O_2		4.7×10^{-5}	25/22	1.270	5.42	0.077	5.9×10^{-5}	5.1×10^{-5}	--	5.2×10^{-5}	4.8×10^{-5}	4.5×10^{-5}
34	O_2		5.0×10^{-5}	21/20	----	1.42	0.10	5.0×10^{-5}	1.0×10^{-5}	8.6×10^{-6}	7.2×10^{-6}	-	
37	O_2		3.0×10^{-4}	33/28	1.281	11.15	0.60	2.8×10^{-4}	----	-	1.9×10^{-4}		1.6×10^{-4}

...ance—N_2 and O_2

Scatter (Beam, deg 6	12	16	Remarks
1 1.4 x 10^{-4}	1.25 x 10^{-4}	1.15 x 10^{-4}	7.8 x 10^{-5}	Diffuse appearance
2.1 x 10^{-6}			--	Purged to 40°K prior to deposition, some residual scatter after purge
3.0 x 10^{-6}			--	Same as 18, rough, diffuse appearance
7.4 x 10^{-6}		8.9 x 10^{-6}	8.2 x 10^{-6}	Deposit added to 19
4.4 x 10^{-6}	4.0 x 10^{-6}	4.3 x 10^{-6}	2.9 x 10^{-6}	Purged to 130°F prior to deposition, diffuse appearance
1.4 x 10^{-5}	1.2 x 10^{-5}	1.3 x 10^{-5}	9.6 x 10^{-6}	Same as 22
4.9 x 10^{-6}	4.1 x 10^{-6}	4.7 x 10^{-6}	3.7 x 10^{-6}	Same as 22
2.0 x 10^{-3}	2.4 x 10^{-3}	3.8 x 10^{-3}	4.7 x 10^{-3}	Same as 18
3.9 x 10^{-6}	3.5 x 10^{-6}	4.5 x 10^{-6}	2.8 x 10^{-6}	Purged to 130°F prior to deposition, diffuse appearance
6.4 x 10^{-6}	6.8 x 10^{-6}	6.8 x 10^{-6}	7.2 x 10^{-6}	Added to 25
2.8 x 10^{-5}	2.9 x 10^{-5}	4.5 x 10^{-5}	3.7 x 10^{-5}	Added to 20, rough, diffuse appearance
1.4 x 10^{-5}	1.4 x 10^{-5}	1.3 x 10^{-5}	1.2 x 10^{-5}	Purged to 130°F prior to deposition, diffuse appearance
4.8 x 10^{-4}	4.2 x 10^{-4}	3.4 x 10^{-4}	2.8 x 10^{-4}	Purged to 50°K prior to deposition
5.4 x 10^{-6}	5.4 x 10^{-6}	3.9 x 10^{-6}	4.2 x 10^{-6}	Same as 31
1.2 x 10^{-6}	8.8 x 10^{-7}	5.3 x 10^{-7}	3.6 x 10^{-7}	
4.8 x 10^{-5}	4.5 x 10^{-5}	4.5 x 10^{-5}	4.1 x 10^{-5}	Purged to 150°F prior to deposition
		5.7 x 10^{-6}	5.0 x 10^{-6}	Purged to 50°. prior to deposition
	1.6 x 10^{-4}		1.1 x 10^{-4}	Invalid scatter data, mirror had particulate contamination